VILNIAUS UNIVERSITETAS

MATEMATIKOS IR INFORMATIKOS FAKULTETAS

Magistro Darbas

Funkcinio gylio klasifikavimo metodai ir taikymai fNIRS duomenims

Functional depth-based supervised classification and application for fNIRS data

Ieva Baliukevičiūtė

VILNIUS 2020

MATEMATIKOS IR INFORMATIKOS FAKULTETAS

TAIKOMOSIOS MATEMATIKOS INSTITUTAS

Darbo vadovas doc. dr. Jurgita Markevičiūtė ______________
(parašas)

Darbo recenzentas dokt. Jovita Gudan

Darbas apgintas 2020 m. sausio mėn. 13 d.

Darbas įvertintas ______________________________________

Registravimo Nr. ______________________________________

Gavimo data 2020 m. sausio mėn. ____ d.

Funkcinio gylio klasifikavimo metodai ir taikymai fNIRS duomenims

Santrauka

Lyčių skirtumai yra plačiai nagrinėjami neurobiologiniu požiūriu. Neurobiologai teigia, kad lyčių sąmoningi bei nesąmoningi informacijos apdorojimo mechanizmai skiriasi. Todėl lytis yra laikoma įtakos turinčiu faktoriumi, lemiančiu kognityvinio eksperimento rezultatus, gautus naudojant fNIRS metodą. Šiame darbe pristatomas funkcinio gylio klasifikavimo algoritmas siekiant atskirti vyrus ir moteris remiantis tik smegenų aktyvumo duomenimis. Siūloma procedūra apima maksimalaus gylio klasifikavimo metodą, kuriame yra keičiami penki skirtingi gylio apibrėžimai norint palyginti gautus rezultatus tarpusavyje. Gauti klasifikavimo rezultatai leidžia manyti, kad hemodinaminis atsakas yra skirtingas tarp lyčių. Be to, ryškiausi skirtumai pastebėti analizuojant kairiojo smegenų pusrutulio duomenis, todėl rezultatai neprieštarauja esamų tyrimų išvadoms.

Raktiniai žodžiai: funkcinių duomenų analizė, funkcinis gylis, funkcinis klasifikavimas, funkcinis gylio klasifikavimas, maksimalaus gylio klasifikavimas, duomenų glodinimas

Functional depth-based supervised classification and application for fNIRS data

Abstract

Gender differences are widely studied from a neurobiological point of view. Neurobiologists argue that gender's conscious and unconscious mechanisms of information processing are different. Thus, gender is considered as an influencing factor for the results of the cognitive experiment obtained using the fNIRS method. The functional depth-based classification algorithm is introduced to discern women and men considering brain activity data. The proposed procedure involves maximum depth-based classification approach while also comparing the results of five different functional depth notions. The results of the proposed method applied for fNIRS data imply that hemodynamic response is different between genders. The main differences can be found in the left brain frontal lobe which follows the knowledge of gender influence to existing cognitive studies.

Key words: functional data analysis, functional depth, functional classification, depth-based classification, maximum depth classifier, data smoothing

Contents

Introduction 7

1 Literature review 7
- 1.1 Statistical depth function . . . 7
- 1.2 Statistical functional depth . . . 9
- 1.3 Functional depth notions . . . 10
  - 1.3.1 The Fraiman and Muniz depth . . . 10
  - 1.3.2 The h-mode depth . . . 11
  - 1.3.3 The random Tukey depth . . . 11
  - 1.3.4 The random projection depth . . . 11
  - 1.3.5 The double random projection depth . . . 12
- 1.4 Depth-based classification . . . 12

2 Functional data analysis framework 13
- 2.1 Data smoothing . . . 13
- 2.2 Descriptive analysis . . . 14

3 Background study 15
- 3.1 Optical Brain Spectroscopy . . . 15
- 3.2 Data collection . . . 16
  - 3.2.1 fNIR400 system . . . 16
  - 3.2.2 Berg Card Sorting Test . . . 17

4 Empirical results 18
- 4.1 fNIRS dataset . . . 18
- 4.2 Data smoothing . . . 20
- 4.3 Descriptive analysis . . . 21
- 4.4 Classification algorithm . . . 23

Conclusions 29

Appendices 34

A Confusion matrices of the classification algorithm 34

B Confusion matrices of k-NN classifier 35

C Performance of k-NN classifier 35

D Algorithm of depths ensemble 37

List of Figures

1 Overview of fNIR device system and sensor pad. 16
2 The stimulus presented on each card had three attributes including shape, colour and number of figures. Each reference card shared one attribute with the target card. Sorting rule of the first match is by number of figures, second - by colour, third - by shape. 17
3 Overview of features measured of 10th woman. 19
4 Overview of features measured of 10th man. 19
5 Raw HBO data of all respondents measured with first optode. The plot on the top represents data for all women participated in the experiment, plot on the bottom - data for all men. 20
6 Smoothed HBO data of all respondents measured with first optode. The plot on the top represents data for all women participated in the experiment, plot on the bottom - data for all men. 21
7 Mean functions of HBO first optode for women and men participated in the experiment. 22
8 Depth functions of HBO first optode for women and men participated in the experiment. 23

List of Tables

1 The structure of modified BCST blocks. 18
2 Percentage of tied classification results. Highlighted cells represent values greater or equal to 20. 26
3 Sensitivity (true positive rates) - rates of correctly classified men. Highlighted cells represent values where percentage of tied classification is greater or equal to 20. 27
4 Specificity (true negative rates) - rates of correctly classified women. Highlighted cells represent values where percentage of tied classification is greater or equal to 20. 27
5 Accuracy results (proportion of correctly classified observations). Highlighted cells represent values where percentage of tied classification is greater or equal to 20. 28
6 F1 scores (harmonic mean of classification precision and sensitivity). Highlighted cells represent values where percentage of tied classification is greater or equal to 20. 28
A.7 Confusion matrices of classification results with all possible combinations of feature, depth and optodes group. M - men, W - women, T - ties. 34
B.8 Confusion matrices of k-NN classification results with all possible combinations of feature and optodes group. M - men, W - women, T - ties. 35
C.9 Percentage of tied classification results with k-NN classifier. Highlighted cells represent values greater or equal to 20. 35
C.10 Sensitivity (true positive rates) - rates of correctly classified men - of k-NN classifier. Highlighted cells represent values where percentage of tied classification is greater or equal to 20. 35
C.11 Specificity (true negative rates) - rates of correctly classified women - of k-NN classifier. Highlighted cells represent values where percentage of tied classification is greater or equal to 20. 35
C.12 Accuracy results (proportion of correctly classified observations) with k-NN classifier. Highlighted cells represent values where percentage of tied classification is greater or equal to 20. 36
C.13 F1 scores (harmonic mean of classification precision and sensitivity) of k-NN classifier. Highlighted cells represent values where percentage of tied classification is greater or equal to 20. 36

List of Algorithms

1 Maximum depth based supervised classification algorithm with leave-one-out schema. 24
2 Final prediction by majority voting rule. 25
D.3 Extension of the classification procedure with depths ensemble. 37

Abbreviations

BCST Berg Card Sorting Test.

FDA Functional data analysis.

FM Fraiman and Muniz depth.

fNIRS Functional Near Infrared Spectroscopy.

HBO Oxyhemoglobin.

HBR Deoxyhemoglobin.

HBT Total blood indraught.

HD Halfspace depth.

hM h-mode depth.

kNN k-nearest neighbours.

MHD Mahalanobis depth.

OXY Oxygenation.

RP Random projection depth.

RPD Double random projection depth.

RT Random Tukey depth.

SD Simplicial depth.

WCST Wisconsin Card Sorting Test.

Introduction

Gender differences are widely studied from a neurobiological point of view. Neurobiologists argue that gender's conscious and unconscious mechanisms of information processing are different. Due to the quantity of information and variety of interpretations, the influence of gender on research results is often understated or overstated. In this thesis, gender is considered as an influencing factor for the results of the cognitive experiment. Over the last decades, new non-invasive optical imaging methods for brain studies have been developing. Particularly, Functional Near-Infrared Spectroscopy (fNIRS), which is used to obtain data analysed in this paper.

The purpose of this thesis is to conclude whether the hemodynamic response measured during the BCST experiment is different between women and men. Thus, neurophysiological data is explored applying techniques of functional data analysis. In particular, the functional depth-based classification algorithm is introduced to discern women and men considering brain activity data. The proposed procedure involves maximum depth-based classification approach with five different functional depth notions changing in maximum depth classifier for comparison.

The thesis is organised as follows: theoretical background is covered in Section 1, with the definitions of statistical depth function 1.1 and statistical functional depth 1.2, review of considered functional depth notions 1.3 and theoretical framework of supervised functional classification 1.4. Section 2 presents theoretical concepts and mathematical background of functional data analysis. Section 3 provides basic knowledge in the domain of neurobiology and explains essentials of neurobiological study conducted to explore gender differences, the section is highly based on Činčiūtė [65]. Section 4 presents empirical work done in this thesis. Results are provided in the appendices: confusion matrices A of the proposed classification algorithm applied for fNIRS dataset, confusion matrices B and performance C of k-NN classification procedure applied for fNIRS dataset. The formal algorithm of depths ensemble is presented in the appendix D.

1 Literature review

1.1 Statistical depth function

Statistical depth is powerful data analytics and nonparametric inference tool for multivariate data. Depth can reveal underlying distribution features such as asymmetry, shape and spread [41]. The objective of statistical depth is to provide a natural centre-outward ordering and a measure of centrality for a multivariate data setting. More formally, depth function is any function $D(x, P)$ which provides a P-based ordering of points $x \in \mathbb{R}^d$ from a depth-based centre outwards with respect to a distribution P in $\mathbb{R}^d$. Furthermore, depth associates a measure of centrality to each point $x \in \mathbb{R}^d$. In 1975, Tukey [58] proposed statistical depth as the analogous definition of univariate rank and order statistics for a multivariate setting. Furthermore, the depth term substitutes the absence of the notion of quantiles in the multivariate context [55].

Depth functions have been vastly explored in the literature. The term was introduced in Tukey [58] as the *halfspace depth*, or *Tukey depth*. The halfspace depth (HD) of a point $x \in \mathbb{R}^d$ with respect to a distribution P in $\mathbb{R}^d$ is the minimum probability carried by any closed halfspace H with x:

$$HD(x, P) = \inf_H \{\mathbb{P}(H : x \in H)\}, \quad x \in \mathbb{R}^d.$$

Definition of *simplicial depth* was proposed in Liu [42]. The simplicial depth (SD) of a point $x \in \mathbb{R}^d$ with respect to a distribution P in $\mathbb{R}^d$ is the probability that x belongs to a random simplex in $\mathbb{R}^d$:

$$SD(x, P) = \mathbb{P}(x \in S[X_1, \ldots, X_{d+1}]), \quad x \in \mathbb{R}^d,$$

where $X_1, \ldots, X_{d+1}$ is a random sample of independent observations from the distribution P and $S[X_1, \ldots, X_{d+1}]$ is the d-dimensional simplex with vertices $X_1, \ldots, X_{d+1}$, that is, the set of all points in $\mathbb{R}^d$ which are convex combinations of $X_1, \ldots, X_{d+1}$.

Liu and Singh [43] suggested definition of *Mahalanobis depth* based on *Mahalanobis distance* [47]. Let $d_{\Sigma_P}(x, \mu_P)$ be the Mahalanobis distance between x and μ_P in $\mathbb{R}^d$, that is, $d_{\Sigma_P}(x, \mu_P) = (x - \mu_P)^T \Sigma_P^{-1}(x - \mu_P)$. Then Mahalanobis depth (MHD) with respect to the distribution function P in $\mathbb{R}^d$ is

$$\begin{aligned} MHD(x, P) &= \left[1 + d_{\Sigma_P}(x, \mu_P)\right]^{-1} \\ &= \left[1 + \left(x - \mu_P\right)^T \Sigma_P^{-1} \left(x - \mu_P\right)\right]^{-1}, \quad x \in \mathbb{R}^d, \end{aligned}$$

where μ_P and Σ_P are the mean and covariance matrix of P respectively. However, MHD leads to nonrobust procedures since μ_P is not a robust statistic as noted in Liu and Singh [43].

Numerous alternative examples of depth have been discussed in the literature. Liu and Singh [43] considered the above mentioned HD, SD, MHD and the *majority depth* in developing a *quality index* for use in connection with manufacturing processes. Koshevoy and Mosler [39] proposed *zonoid* depth function based on *zonoid trimming*. Bartoszyński et al. [6] suggested a depth approach based on interpoint distances in the context of a multivariate goodness-of-fit test. Rousseeuw and Hubert [54] introduced *regression depth*. Vardi and Zhang [60] defined a method for constructing depth functions from notions of multivariate median. Zuo and Serfling [64] formulated non-parametric notions of multivariate *scatter measure* based on general depth functions.

However, most of these works have been introduced without concern to whether they fulfil a particular set of criteria. Statistical depth functions lacked a formal definition of its properties until Zuo and Serfling [63]. Following the spirit of Liu [42], definition of statistical depth function was formalised in Zuo and Serfling [63] under the Definition 1.1.1.

Definition 1.1.1 (Zuo and Serfling [63]). *Let $\mathcal{P}$ denote the class of distributions on the Borel sets of $\mathbb{R}^d$ and $P = P_X$ denote the distribution of a given random vector X. The bounded and non-negative mapping $D(\cdot, \cdot) : \mathbb{R}^d \times \mathcal{P} \to \mathbb{R}$ is called a* statistical depth function *if it satisfies the following properties:*

(P1) Affine invariance. *$D(Ax + b, P_{AX+b}) = D(x, P_X)$ holds for any random vector X in $\mathbb{R}^d$, any $d \times d$ non-singular matrix A and any $b \in \mathbb{R}^d$, where P_X denotes the distribution of X and P_{AX+b} denotes the distribution of $AX + b$.*

(P2) Maximality at centre. *$D(\theta, P) = \sup_{x \in \mathbb{R}^d} D(x, P)$ holds for any $P \in \mathcal{P}$ having a unique centre of symmetry θ with respect to some notion of symmetry.*

(P3) Monotonicity relative to the deepest point. *For any $P \in \mathcal{P}$ having the deepest point θ, $D(x, P) \le D(\theta + \alpha(x - \theta), P)$ hold for all $\alpha \in [0, 1]$.*

(P4) Vanishing at infinity. *$D(x, P) \to 0$ as $\|x\| \to \infty$, for each $P \in \mathcal{P}$, where $\|\cdot\|$ is the Euclidean norm.*

1.2 Statistical functional depth

In fields such as financial markets and medicine, more complex high-dimensional data arise and the use of functional data is preferable [53]. Therefore, the demand for inference tools for infinite-dimensional or functional data has increased. Efforts to extend multivariate statistical depth constructions to the functional context have been demonstrated in the literature. Cuevas et al. [16] indicate that considerable room for further research exists, regardless of the recent progress in the field. As described in Nieto-Reyes and Battey [50], it is not straightforward, whereas direct extensions of multivariate depth, designed to satisfy properties in multivariate space, neglect the shape and structure properties of functional data.

Despite attempts at extending the notion of multivariate statistical depth to the functional setting, a formal definition of statistical functional depth was absent. The need for an explicit definition and absence of one was first pointed out in Nieto-Reyes [49], where the first attempt to address the problem was made. Nevertheless, the most evident formalisation of statistical functional depth was presented in Nieto-Reyes and Battey [50]. The properties that constitute the Definition 1.2.2 provide a sophisticated extension of properties defining the multivariate statistical depth (Definition 1.1.1), recognising topological features such as continuity, contiguity and smoothness. The Definition 1.2.2 relies on the following preliminary Definition 1.2.1 of the convex hull.

Let us introduce notation used in Definition 1.2.1 and Definition 1.2.2. $\mathcal{H}$ denotes a Hilbert space with compact support $\mathcal{V}$, $(\mathcal{H}, d)$ is a separable metric space and $\mathcal{A}$ is the σ-algebra on $\mathcal{H}$ generated by the open d metric balls for some metric $d(\cdot,\cdot)$ on $\mathcal{H}$. Separability of $(\mathcal{H}, d)$ guarantees that $\mathcal{A}$ coincides with the Borel σ-algebra on $\mathcal{H}$ [59, Chapter 1.7].

Definition 1.2.1 (Nieto-Reyes and Battey [50]). *Let $(\mathcal{H}, \mathcal{A}, P)$ be a probability space, where $P \in \mathcal{P}$, the space of all probability measures on $\mathcal{H}$. Define $\mathcal{E}$ to be the smallest set in the σ-algebra $\mathcal{A}$ such that $P(\mathcal{E}) = P(\mathcal{H})$. Then the* convex hull *of $\mathcal{H}$ with respect to P is defined as*

$$\mathcal{C}(\mathcal{H}, P) = \{x \in \mathcal{H} : x(v) = \alpha L(v) + (1-\alpha)U(v) : v \in \mathcal{V}, \alpha \in [0,1]\},$$

where $U = \{\sup_{x\in\mathcal{E}} x(v) : v \in \mathcal{V}\}$ and $L = \{\inf_{x\in\mathcal{E}} x(v) : v \in \mathcal{V}\}$.

Definition 1.2.2 (Nieto-Reyes and Battey [50]). *Let $(\mathcal{H}, \mathcal{A}, P)$ be a probability space as in Definition 1.2.1. Let $\mathcal{P}$ be the space of all probability measures on $\mathcal{H}$. The bounded and non-negative mapping $D(\cdot,\cdot) : \mathcal{H} \times \mathcal{P} \to \mathbb{R}$ is called a* statistical functional depth *if it satisfies the following properties:*

(F1) Distance invariance. *$D(f(x), P_{f(X)}) = D(x, P_X)$ for any $x \in \mathcal{H}$ and $f : \mathcal{H} \to \mathcal{H}$ such that for any $y \in \mathcal{H}$, $d(f(x), f(y)) = a_f \cdot d(x, y)$, with $a_f \in \mathbb{R} \setminus \{0\}$.*

(F2) Maximality at centre. *For any $P \in \mathcal{P}$ possessing a unique centre of symmetry $\theta \in \mathcal{H}$ with respect to some notion of functional symmetry, we have $D(\theta, P) = \sup_{x\in\mathcal{H}} D(x, P)$.*

(F3) Strictly decreasing with respect to the deepest point. *For any $P \in \mathcal{P}$ such that $D(z, P) = \max_{x\in\mathcal{H}} D(x, P)$ exists, $D(x, P) < D(y, P) < D(z, P)$ holds for any $x, y \in \mathcal{H}$ such that $\min\{d(y, z), d(y, x)\} > 0$ and $\max\{d(y, z), d(y, x)\} < d(x, z)$.*

(F4) Upper semi-continuity in x. *$D(x, P)$ is upper semi-continuous as a function of x, that is, for all $x \in \mathcal{H}$ and all $\epsilon > 0$, there exists a $\delta > 0$ such that*

$$\sup_{y:d(x,y)<\delta} D(y, P) \le D(x, P) + \epsilon.$$

(F5) Receptivity to convex hull width across the domain. *$D(x, P_X) < D(f(x), P_{f(X)})$ for any $x \in \mathcal{C}(\mathcal{H}, P)$, as in Definition 1.2.1, with $D(x, P) < \sup_{y \in \mathcal{H}} D(y, P)$ and $f : \mathcal{H} \to \mathcal{H}$ such that $f(y(v)) = \alpha(v)y(v)$ with $\alpha(v) \in (0, 1)$ for all $v \in L_\delta$ and $\alpha(v) = 1$ for all $v \in L_\delta^c$, where*

$$L_\delta = \arg\sup_{H \subseteq \mathcal{V}} \Big\{ \sup_{x,y \in \mathcal{C}(\mathcal{H},P)} d(x(H), y(H)) \leq \delta \Big\}$$

for any $\delta \in \big[\inf_{v \in \mathcal{V}} d(L(v), U(v)), d(L, U)\big]$ such that $\lambda(L_\delta) > 0$ and $\lambda(L_\delta^c) > 0$. Here λ denotes Lebesgue measure on $\mathcal{V}$.

(F6) Continuity in P. *For all $x \in \mathcal{H}$, for all $P \in \mathcal{P}$ and for every $\epsilon > 0$, there exists a $\delta(\epsilon) > 0$ such that $|D(x, Q) - D(x, P)| < \epsilon$ P-almost surely for all $Q \in \mathcal{P}$ with $d_{\mathcal{P}}(Q, P) < \delta$ P-almost surely, where $d_{\mathcal{P}}$ metricises the topology of weak convergence.*

Alternative property to (F2) was considered in Nieto-Reyes and Battey [50], as unique notion of symmetry is absent even in the multivariate case. Property (F2G) is a direct extension of (P2) from the multidimensional context towards functional setting.

(F2G) Maximality at Gaussian process mean. *For P a zero-mean, stationary and almost surely a Gaussian process on $\mathcal{V}$, $D(\theta, P) = \sup_{x \in \mathcal{H}} D(x, P) \neq \inf_{x \in \mathcal{H}} D(x, P)$, where θ is the zero mean function.*

The formalisation of the properties functional depth should meet is more complex than in the multivariate case. Yet, ideas presented in Nieto-Reyes and Battey [50] have not reached similar recognition as widely acknowledged Definition 1.1.1 of statistical depth function for the multivariate setting. Citing directly from Gijbels and Nagy [29], it is demonstrated that the conditions needed for some desirable properties to hold are extremely demanding, and virtually impossible to be met for common depths. Hence, further insights have to be gained and properties might need reformulation. To be precise, the condition (F1) was found difficult to achieve for some functional depth approaches. Nonetheless, invariance properties are required to use depth notion as an analytical tool for comparison between distributions. Requirement (F5) is rational in some applications concerning measurement error. However, (F5) is too restrictive and can lead to missing valuable insight into the nature of the analysed process.

1.3 Functional depth notions

Various functional depth approaches have been introduced in the literature since the appearance of the first functional depth in Fraiman and Muniz [27]. To be specific, several constructions that have appeared in the literature are the *integrated dual depth* in Cuevas and Fraiman [15], the (modified) *band depth* and the (modified) *half region depth* in López-Pintado and Romo [45, 46], and the functional version of *spatial depth* in Chakraborty and Chaudhuri [9, 10].

In this paper, five statistical functional depth approaches are considered. Particularly, the Fraiman and Muniz depth, the h-mode depth, the random Tukey depth, the random projection depth and the double random projection depth. Here each of the depth constructions will be discussed in more detail.

1.3.1 The Fraiman and Muniz depth

The first depth for functional data was proposed in Fraiman and Muniz [27]. The Fraiman and Muniz (*FM*) method is based on integrated depth.

Let $X_1(t), \dots, X_n(t)$ be independent and identically distributed stochastic processes with respect to the the univariate marginal distribution P_n. Let D_n be any depth concept, say simplicial depth (see Section 1.1), defined on $\mathbb{R}$. For every fixed $t \in [0,1]$ the univariate depth of $X_i(t)$ at t with respect to $X_1(t), \dots, X_n(t)$ is considered as $D_n(X_i(t)) = Z_i(t)$. Then, at each single point t the values $X_1(t), \dots, X_n(t)$ are ranked according to their depths $Z_i(t)$, where $i = 1, \dots, n$.

The FM depth method is based on defining

$$I_i = \int_0^1 Z_i(t)dt, \quad 1 \leq i \leq n. \tag{1}$$

Thus, functions $X_1(t), \dots, X_n(t)$ are ranked according to values of I_i derived from (1) to obtain order statistics $X^{(1)}(t), \dots, X^{(n)}(t)$, where $X^{(1)}(t)$ denote the deepest function or functional median, for which I_i is maximum.

1.3.2 The h-mode depth

The h-mode (hM) depth notion, introduced in Cuevas et al. [16], is based on average of the kernelized distances using the L_2 norm to denote the deepest function.

Let $(\mathcal{H}, d) = (\mathbb{H}, \|\cdot\|_{L_2})$, the hM depth at $x \in \mathbb{H}$ with respect to the distribution P is given by the function

$$D_h(x, P) = \mathbb{E}(K_h(\|x - X\|_{L_2})), \tag{2}$$

where X is a functional random variable on the probability space $(\mathcal{H}, \mathcal{A}, P)$ and, for fixed $h > 0$, $K_h(\cdot)$ is a re-scaled kernel of type $K_h(\cdot) = \frac{1}{h}K(\cdot/h)$, where $K(\cdot)$ is the Gaussian kernel[1]. The deepest function of x is achieved by maximizing the function (2).

1.3.3 The random Tukey depth

The random Tukey (RT) depth was suggested in Cuesta-Albertos and Nieto-Reyes [12]. The RT approach is a random approximation of Tukey depth or halfspace depth (see Section 1.1) for functional data. The RT method is achieved by obtaining all possible one-dimensional projections of the curves while applying the halfspace depth.

Let $(\mathcal{H}, d) = (\mathbb{H}, \|\cdot\|_{L_2})$ and define $\mathcal{U} = \{u_1, \dots, u_k\}$, where $u_j, j = 1, \dots, k$, are the realisations of $U_j, j = 1, \dots, k$, drawn independently from a non-degenerate probability measure $\mu \in \mathbb{H}$. The RT depth at $x \in \mathbb{H}$ with respect to P is

$$D_{\mathcal{U}}(x, P) = \min_{u \in \mathcal{U}} D_1(\langle u, x \rangle, P_u),$$

where, for every probability measure Q on the Borel sets of $\mathbb{R}$, $D_1(t, Q) = \min\{Q(-\infty, t], Q[t, \infty)\}$, P_u is the marginal of P on $\{\langle u, x \rangle : x \in \mathbb{H}\}$. The RT is a random variable by its nature, therefore values and ordering obtained might be different for the same functional data.

1.3.4 The random projection depth

The random projection (RP) depth was offered in Cuevas et al. [16]. The RP method was inspired by some ideas of Cuesta-Albertos et al. [13, 14].

Let $(\mathcal{H}, d) = (\mathbb{H}, \|\cdot\|_{L_2})$, $X_1, \dots, X_n$ be a sample of functional data and a is a random direction independent from the X_i. The sample depth of X_i is given as the univariate depth

[1] In Cuevas et al. [16], Gaussian kernel is defined as $K(t) = \frac{1}{\sqrt{2\pi}} \exp(\frac{-t^2}{2})$.

of the corresponding one-dimensional projection. Let us assume that X_i belong to Hilbert space $L^2[0,1]$ and projection of a datum X is defined as the standard inner product

$$\langle a, X\rangle = \int_0^1 a(t)X(t)dt. \tag{3}$$

The definition of *RP* depth method is based on the rank of the projections along a random direction, therefore it provides a random measure of a functional depth. Hence, depth of a datum x with respect to a random element X is given as the random quantile $\langle a, x\rangle$ in the distribution of $\langle a, X\rangle$.

1.3.5 The double random projection depth

The double random projection (*RPD*) depth was proposed in Cuevas et al. [16]. The *RPD* method simultaneously applies the random projection approach (see Section 1.3.4) involving functions and its derivatives. Consequently, the information on the function smoothness is incorporated.

Let $X_1, \ldots, X_n$ be a sample of differentiable functions defined on $[0,1]$. In the first step, random projections are built for functions and their derivatives by employing (3). That is, the sample of functions $X_1, \ldots, X_n$ is reduced to a sample in $\mathbb{R}^2$ and defined by $(\langle a, X_1\rangle, \langle a, X_1'\rangle), \ldots, (\langle a, X_n\rangle, \langle a, X_n'\rangle)$. In the second step, h-mode depth function (see Section 1.3.2) is applied in order to evaluate the depth of the bi-dimensional projected data. The resulting procedure is denoted as the *RPD* depth.

1.4 Depth-based classification

According to description specified in Ferraty and Vieu [26, Section 8.2], theoretical framework of supervised functional classification is given as follows. Let $(y_i, g_i)_{i=1,\ldots,n}$ be a sample of n observed random pairs, identically and independently distributed as (Y, G), where y_i denote functional random data and g_i are the categorical responses. In binary classification problem, let us assume that g_i can take values 0 or 1. Thus, n_0 observations come from the class with label 0, n_1 observations come from the class with label 1 and $n = n_0+n_1$. In addition, let x be an independent identically distributed as Y curve with unknown class membership. Using the information contained in $(y_i, g_i)_{i=1,\ldots,n}$, the objective of supervised functional classification method is to provide a rule to classify the observation x and predict the unknown class of x.

Interesting developments surrounding the theory and practice of functional classification problems have been made in the literature. The functional version of multivariate *linear discriminant analysis* has been considered in James and Hastie [37]. The use of nonparametric *kernel estimators* for supervised classification in the functional context has been analysed in Ferraty and Vieu [25]. The extension of the *k-nearest neighbours* (*k-NN*) method for infinite-dimensional data has been provided in Cérou and Guyader [18]. Other functional classification procedures have emerged in the last decade including the *near perfect classification* method in Delaigle and Hall [19], classifiers based on the functional *mixed model* in Zhu et al. [62] and the *componentwise classification* method in Delaigle et al. [20].

As indicated in Helander [32], since depth is a measure of typicality and outlyingness, the depth-based methods are designed to be suitable for datasets that may hold outlying curves. Therefore, the possibility of using functional depth for functional supervised classification problems have been considered. The *distance to the trimmed mean* and *weighted average distance* procedures for functional data classification were introduced in López-Pintado and Romo [44]. More recently, *DD-plot classification* method was proposed in Lange et al. [40].

In this thesis, the *maximum depth classification* procedure is considered. The concept of maximum depth classifiers, first applied in the multivariate context in Ghosh and Chaudhuri

[28], was extended for functional data in Cuevas et al. [16]. The main idea behind the procedure is that depth value of any statistical functional depth notion (see Section 1.3) is evaluated for observation x with respect to the empirical distribution of each class 0 and 1. The observation x is then assigned to the class, where the highest depth of x is achieved. More formally, the within maximum depth classifier in our case can be expressed as

$$C_D(x) = \arg\max_j D_{m_j}(j, x),$$

where m_j denote the number of observations in the training sample from the jth class, $j = 0, 1$, $D_{m_j}(j, x)$ is the empirical depth of x in the training sample of the jth class.

2 Functional data analysis framework

A brief overview of techniques applied in functional data analysis (FDA) framework will be discussed in this section.

In the FDA setting, term *functional* refers to the specific continuous structure of the observed units. Therefore, observed data is considered as representing an underlying function at various locations, and each curve is treated as a single functional entity [53]. Time is the commonly encountered continuum over which the functions may be recorded, but other continuous domain, such as spatial position, frequency and concentration, is possible.

In addition to continuity, a certain level of smoothness from the underlying process generating the data is assumed in the FDA [53]. This assumption means that the function possesses a specific number of derivatives. Hence, the first step, when dealing with functional data, is to smooth observed discrete data to construct an estimate for the functional curve that acquires a suitable number of derivatives. The smoothness of the underlying function might not be apparent from the raw observation vector due to the presence of noise imposed on the signal by the measurement process. The underlying process may be measured on as few as 20 or up to tens of thousands of discrete points on the continuum. Furthermore, the process may also be measured repeatedly: either by multiple samples of a single process (within subjects) or by samples from the process measured in multiple subjects (across subjects). Moreover, adjacent observations are not assumed to be independent in the context of the FDA unlike in traditional multivariate analysis.

2.1 Data smoothing

One of the special characteristics of functional data is that observations can be measured over an arbitrary set of points in time, preventing the direct use of multivariate methods in analysis. Hence, the first step in the FDA is to smooth discrete observed data points to obtain a functional object.

Let t be a one-dimensional argument, say referred to as time. Functions of t are observed over discrete grid $\{t_1, \dots, t_J\} \in \mathcal{T}$ at sampling times t_j, $j = 1, \dots, J$, which are not necessarily equally spaced. The observed data are filled with measurement errors or noise imposed by the underlying signal. Commonly, in the real world problems, N processes are being observed simultaneously. Let y be a vector of N functional data $y = [y_1, \dots, y_N]^T$ and for each functional observation we have

$$y_{ij} = X_i(t_{ij}) + \epsilon_{ij}, \tag{4}$$

where y_{ij} denotes observation of the stochastic process $X_i(t_{ij})$ with the random error ϵ_{ij} of zero mean and variance function σ^2 associated with the ith functional datum. More formally,

$X_i(t)$ is the conditional expectation of y_{ij}, given $t_{ij} = t$. That is,

$$X_i(t) = \mathbb{E}(y_{ij}|t_{ij} = t), \quad i = 1, \dots, N, \quad j = 1, \dots, J_i.$$

Numerous techniques can be applied to smooth the function $X_i(t)$ in (4). In basis expansions, such as Fourier basis, polynomial spline basis and B-spline basis, smoothness is imposed by either restricting the basis or by specifying a roughness penalty. As an alternative, free-knot splines and wavelets provide data-adaptive basis systems. Splines are well suited in the cases when functional derivatives are required. Wavelets are useful for data with sharp peaks.

Functions representation by basis functions

In this paper, representation of functional observations by Fourier basis functions is considered and described following the ideas of Ramsay and Silverman [53]. The sample of curves are assumed to be observations of a stochastic process $X_i = \{X_i(t) : t \in \mathcal{T}\}$ and belong to the Hilbert space L_2 of square integrable functions with the inner product

$$\langle X_1, X_2 \rangle = \int_{\mathcal{T}} X_1(t) X_2(t) dt, \quad \forall X_1, X_2 \in L_2(\mathcal{T}).$$

A basis system needs to be specified to create a smooth functional object. The chosen basis is a linear combination of functions defining the functional observation. As each functional observation in a dataset is typically treated independently the same way, the equation (4) can be simplified. Thus, further in this section $y_j = x(t_j) + \epsilon_j$, $j = 1, \dots, J$, is denoted. The aim of the function reconstruction process is to represent an observation $x(t)$, given $t_j = t$, as a linear expansion of K known basis functions ϕ_k as follows

$$x(t) = \sum_{k=1}^{K} c_k \phi_k(t) = \boldsymbol{c}^T \boldsymbol{\phi}(t), \quad \forall t \in \mathcal{T}, \tag{5}$$

where $\boldsymbol{c} = [c_1, \dots, c_K]$ and $\boldsymbol{\phi}(t) = [\phi_1(t), \dots, \phi_K(t)]$.

Basis functions expansion represent the potentially infinite-dimensional universe of functions within the finite-dimensional framework of vectors $\boldsymbol{c}$. Furthermore, choice of the basis system $\boldsymbol{\phi}(t)$ has a great effect on the smoothness of $x(t)$.

The Fourier basis system

The most suitable basis for periodic data defined on interval $\mathcal{T}$ is the Fourier basis [53]. The Fourier basis functions ϕ_k are given by

$$\phi_0(t) = \frac{1}{\sqrt{|\mathcal{T}|}}, \quad \phi_{2r-1}(t) = \frac{\sin(rwt)}{\sqrt{|\mathcal{T}|/2}}, \quad \phi_{2r}(t) = \frac{\cos(rwt)}{\sqrt{|\mathcal{T}|/2}},$$

for $r = 1, \dots, \frac{K-1}{2}$, where K is the odd number of basis functions. The frequency w determines the period and the length of the interval $|\mathcal{T}| = 2\pi/w$ and the function vector $\phi(t) = [\phi_0(t), \phi_1(t), \dots, \phi_{2r}(t)]^T$ is evaluated at discrete points of time t_j, $j = 1, \dots, J$.

2.2 Descriptive analysis

Exploratory analysis is an important part of data analysis. Functional data are described by functional summary statistics [53].

Mean and variance functions

The mean function is defined as $\mu(t) = \mathbb{E}(x(t))$, $\forall t \in \mathcal{T}$. The sample functional mean is

$$\bar{x}(t) = \frac{1}{N}\sum_{i=1}^{N} x_i(t), \quad \forall t \in \mathcal{T},$$

where N is the number of functional observations or replications and $x_i(t)$ is the ith curve evaluated at time t.

The variance function is defined as $\sigma^2 = \mathbb{E}[x(t) - \mu(t)]^2$, $\forall t \in \mathcal{T}$. The sample functional variance is

$$\mathrm{Var}(x(t)) = \frac{1}{N-1}\sum_{i=1}^{N}(x_i(t) - \bar{x}(t))^2, \quad \forall t \in \mathcal{T}.$$

The standard deviation function is the square root of the variance function.

3 Background study

Interpretation of biological significance of the fact that human brains are split into two hemispheres attracted controversy and led to the emergence of many theories. Though neuroimaging methods became extensively used 30 years ago, asymmetry of brain hemispheres is not completely explained [34, 56, 57]. It is described in Hugdahl and Westerhausen [34] that abnormal brain hemispheric asymmetry is associated with disorders including depression, schizophrenia, bipolar disorder, and dyslexia. Irregular results are often due to an abnormally large degree of asymmetry between the right and left hemispheres following specific damage to one side of the brain.

Gender differences are widely studied from a neurobiological point of view. Goldberg et al. [30], Hugdahl and Westerhausen [34] argue that gender's conscious and unconscious mechanisms of information processing are different. The distribution of the various neurotransmitter receptors in the brain hemispheres is different between women and men. Hugdahl and Westerhausen [34] suggest that the entire brain is being affected not uniformly rather than affection is localized in the specific hemisphere. Činčiūtė [65] points that due to the quantity of information and variety of interpretations, the influence of gender on research results is often understated or overstated. In this thesis, gender is considered as an influencing factor for the results of the cognitive experiment.

3.1 Optical Brain Spectroscopy

Non-invasive brain studies are popular in public healthcare centres and scientific research centres. These studies effectively provide a diagnosis without significant discomfort for patients. Most common are Electroencephalography and Functional Magnetic Resonance Imaging which often are combined to get more informative results.

Over the last decades, new methods based on optical imaging have been developing [38]. These methods are mainly used to research human cognitive abilities. Optical imaging methods have high temporal and spatial resolutions and are more mobile and cheaper. Optical brain spectroscopy is based on light absorption in tissue, which is dependent on the amount of chromophores[2], source omitted light wavelength, tissue thickness and other external factors. This method does not have any side effects or need for ingestion of chemical substances. It

[2]Chromofore is the part of a molecule or a set of atoms which provides some physical characteristic, e.g. colour, to biological compounds [36].

is based entirely on the physical properties of light and knowledge of physiological processes. Optical imaging methods are classified as Diffuse Optical Tomography, Event-Related Optical Signal and Near-Infrared Spectroscopy [8]. Since optical imaging methods are developing, we will focus further on Functional Near-Infrared Spectroscopy (fNIRS) used to obtain data analysed in this paper.

Glucose is the main energy source for neurons. Neuron activation increases glucose metabolism, which raises the need for oxygen in brains, therefore widening of blood vessels. Over the next few seconds, active brain surface tissue is saturated by glucose and oxyhemoglobin. Concentrations of oxyhemoglobin and deoxyhemoglobin are directly measured in fNIRS.

The fNIRS is a recognized method in the neurobiologists community. It is flexible and convenient tool with wide possibilities for application. The method is often used in pediatrics [7, 11, 33]. Moreover, there is a high interest in fNIRS application to diagnose mental diseases [17, 22, 24].

3.2 Data collection

3.2.1 fNIR400 system

In this paper, we use the hemodynamic response data collected with fNIR400 (Continuous Wave Functional Near-Infrared Spectroscopy) device by Činčiūtė [65]. The hemodynamic response is recorded using magnetic resonance or optical infrared functional brain imaging methods. This measure is associated with changes in neuron activity. The fNIR400 device system consists of data gathering and transmitting system block, sensor, monitoring computer, software "COBI" and data analysis software "fnirSoft" [1]. The sensor pad is designed for frontal brain zone and is placed on a hairless forehead area while fixed on the back of the head (Figure 1).

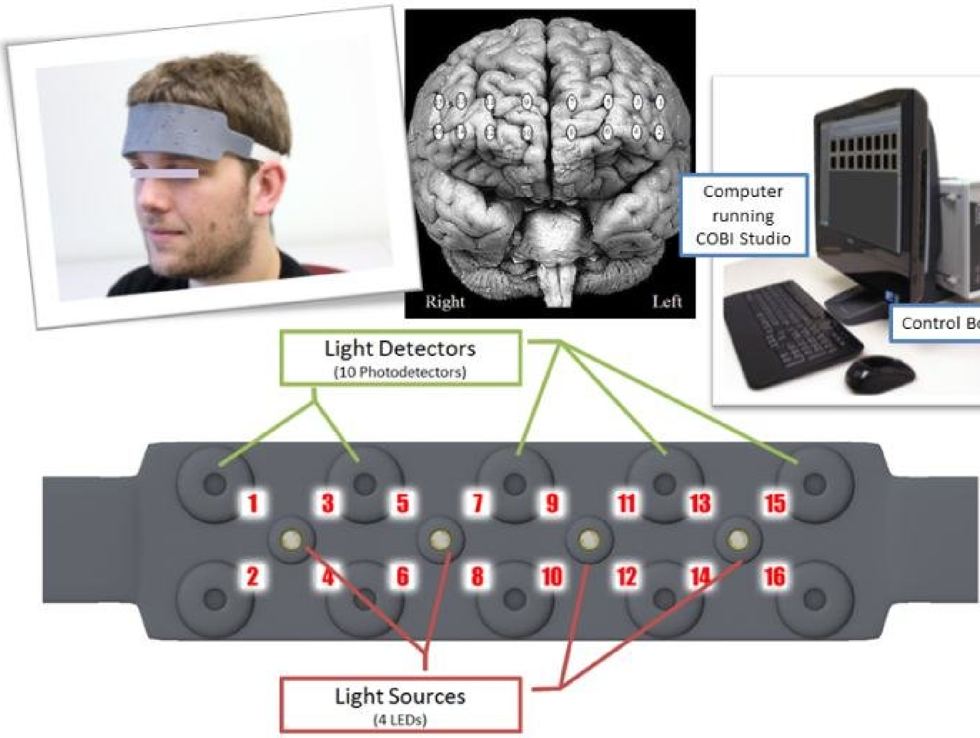

Figure 1: Overview of fNIR device system and sensor pad.
Source: Ayaz et al. [4, page 4]

Optode is a pair of light source and detector. There are 16 optodes in total on a sensor pad. One optode can simultaneously measure 3 wavelengths. Raw data is transformed into 4 features by Beer-Lambert Law [35]:

a) Oxyhemoglobin (HBO);

b) Deoxyhemoglobin (HBR);

c) Oxygenation (OXY = HBO - HBR);

d) Total blood indraught (HBT = HBO + HBR).

3.2.2 Berg Card Sorting Test

During the experiment brain frontal lobe stimulation is induced by Berg Card Sorting Test (BCST)[3]. The BCST is a known neurobiological method to diagnose damage in brain frontal lobe [48, 51]. Human personality is formed in brain frontal lobe. Due to complex activity in brain frontal lobe, common cognitive tests are not able to show possible brain disorders. During the card sorting exercise, both hemispheres of brain frontal lobe are being activated. Consequently, the stability of a patient's cognitive functions can be evaluated [52]. Ordinary BCST card deck consists of 128 cards which differ in shape, colour and number of figures. Patient's speed, accuracy and rule comprehension are monitored during the exercise. In this paper, the BCST was used only for brain stimulation to obtain hemodynamic fluctuations. Respondent's answers were not taken into account in the analysis.

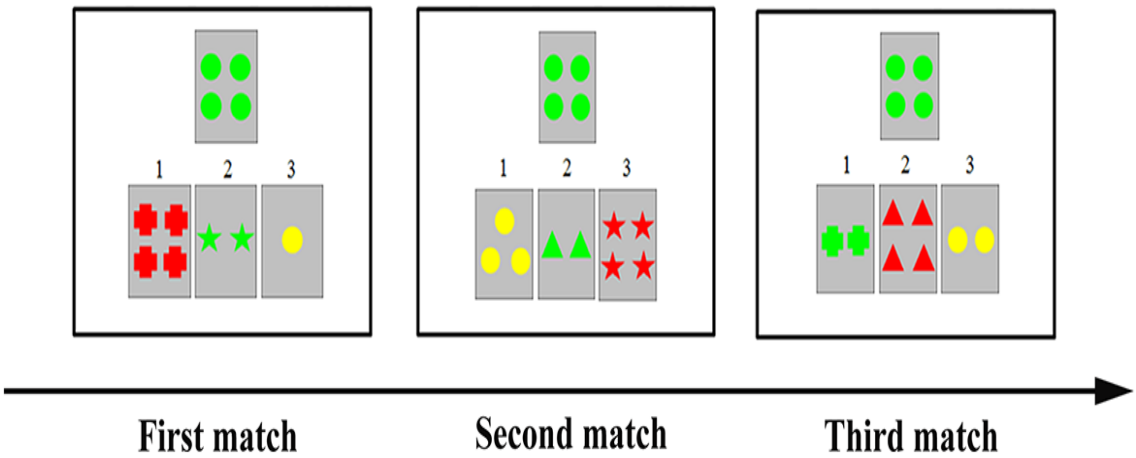

Figure 2: The stimulus presented on each card had three attributes including shape, colour and number of figures. Each reference card shared one attribute with the target card. Sorting rule of the first match is by number of figures, second - by colour, third - by shape.
Source: Wang et al. [61]

During the test, the respondent had to sort card deck by colour, shape and number of figures (Figure 2). Sorting rule changes without informing the respondent. To eliminate changes in brain activity influenced by a test's visual stimulation itself, BCST was modified in four blocks (Table 1). Each block is separated by a 30-second break to suppress hemodynamic fluctuations after the performed exercise.

The first block "Training" is to teach the respondents the rules of the sorting test. The second ("1st control") and the last blocks ("2nd control") are the same and are used to

[3]BCST is also called the Wisconsin Card Sorting Test (WCST). The latter is a BCST with a different rule of points count [21].

	Training	1st control	BCST	2nd control
Number of cards	24	64	128	64
Number of rules	3	1*	3	1*

Table 1: The structure of modified BCST blocks.
Source: Činčiūtė [65, page 34]
* The same sorting rule was applied in control blocks.

identify the hemodynamic response of the main experiment - third block ("BCST"). All obtained data is stored by the software.

4 Empirical results

In this section fNIRS data collected applying techniques described in Section 3 is considered. The data structure is outlined with in-depth explanation and visualisations in Section 4.1. The approach applied to smooth discrete data points of the fNIRS dataset to obtain a smooth functional data object is defined in Section 4.2. Functional data is described by providing visualisations of mean and depth functions in Section 4.3. Finally, the classification is conducted by classification algorithm introduced in section 4.4. `R` packages with suitable routines for exploratory and descriptive analysis of functional data, namely `fda` [2] and `fda.usc` [3, 23], were used to perform the analysis further.

4.1 fNIRS dataset

Data of the main BCST experiment is considered in further analysis. The analysed dataset depicts the hemodynamic response measurements of 35 women and 35 men during the test. All of the 70 selected respondents are similar age and education level to achieve sample as homogeneous as possible.

Changes in the concentration of oxyhemoglobin and deoxyhemoglobin as well as oxygenation and total blood indraught are measured during the test. In Figure 3 raw data of one woman observed during the experiment is represented. Likewise, in Figure 4 data of one man is demonstrated for comparison. In both cases, each curve corresponds to the hemodynamic response measured by an optode. Moreover, curves of optodes tend to get a similar trend under each feature. This tendency may be influenced by biological mechanisms like breathing. Thus, the absence of explanatory variables about these mechanisms constrains further analysis. Therefore, the assumption that data is not under such influence is made.

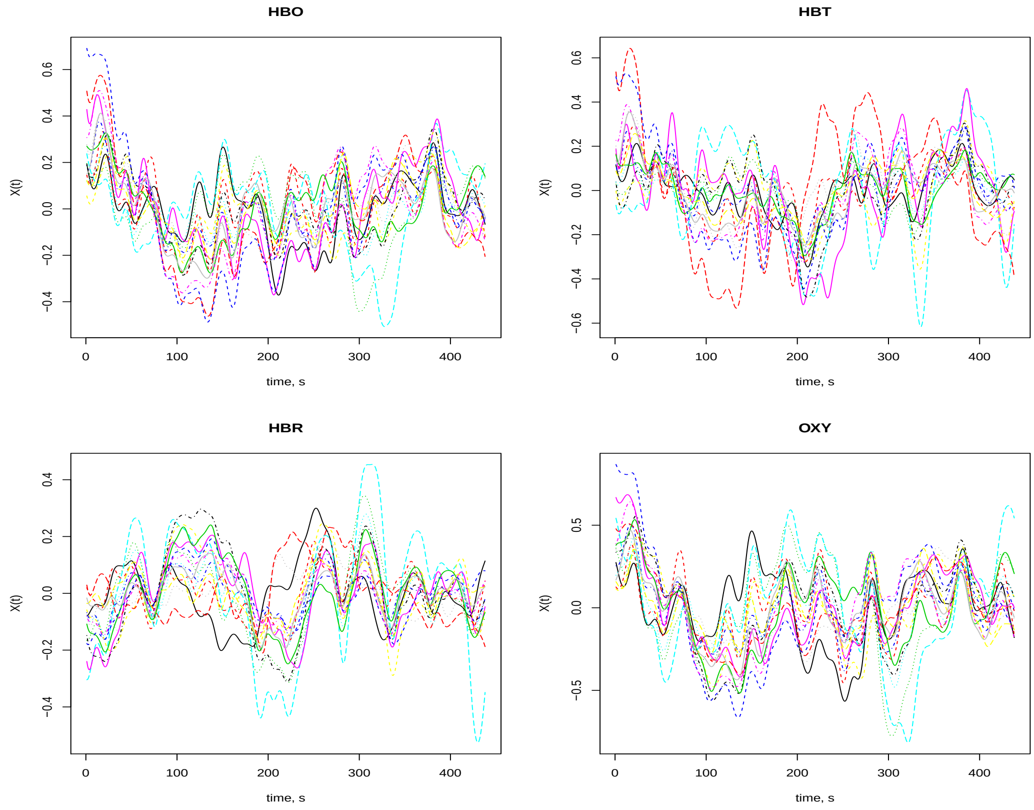

Figure 3: Overview of features measured of 10th woman.
Source: created by the author.

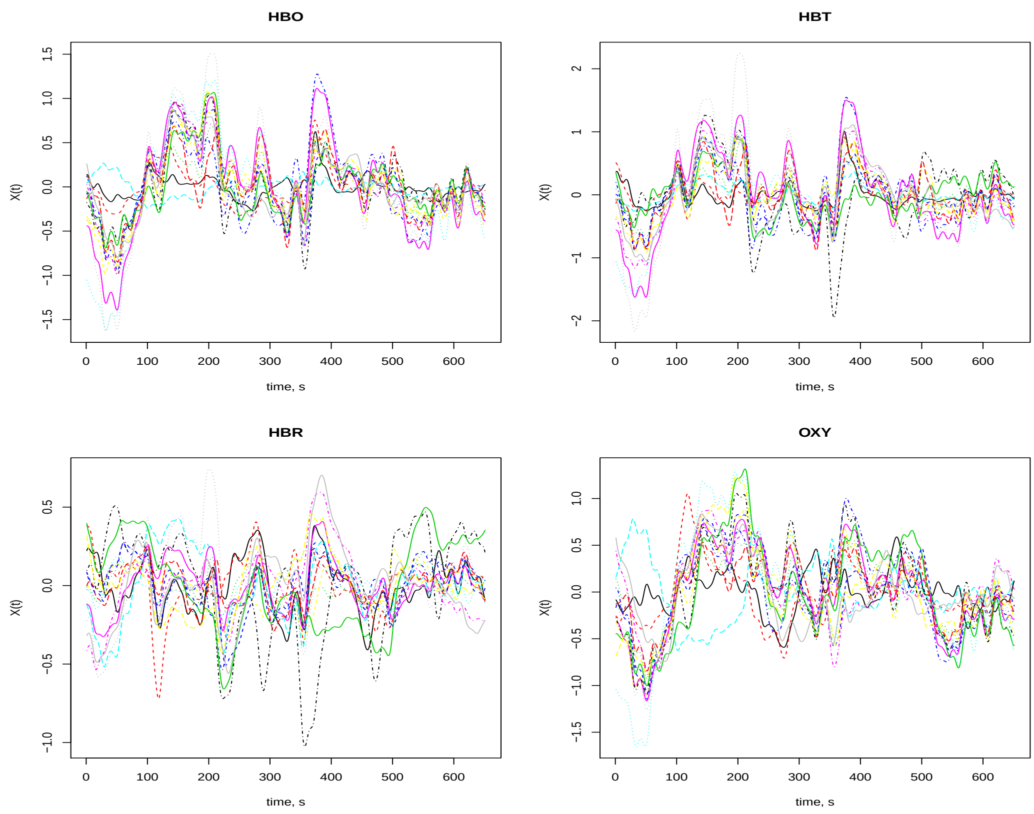

Figure 4: Overview of features measured of 10th man.
Source: created by the author.

The difference in observed time lengths, amount of local minima and maxima, and amplitude variations are fundamental obstacles related to fNIRS data and are visible in Figure 5. These issues occur for the reason that respondents tend to react to the exercise differently (get excited easily or act calmly). Although a sample of respondents is quite homogeneous, cognitive abilities among them may differ as well as the duration they complete the exercise.

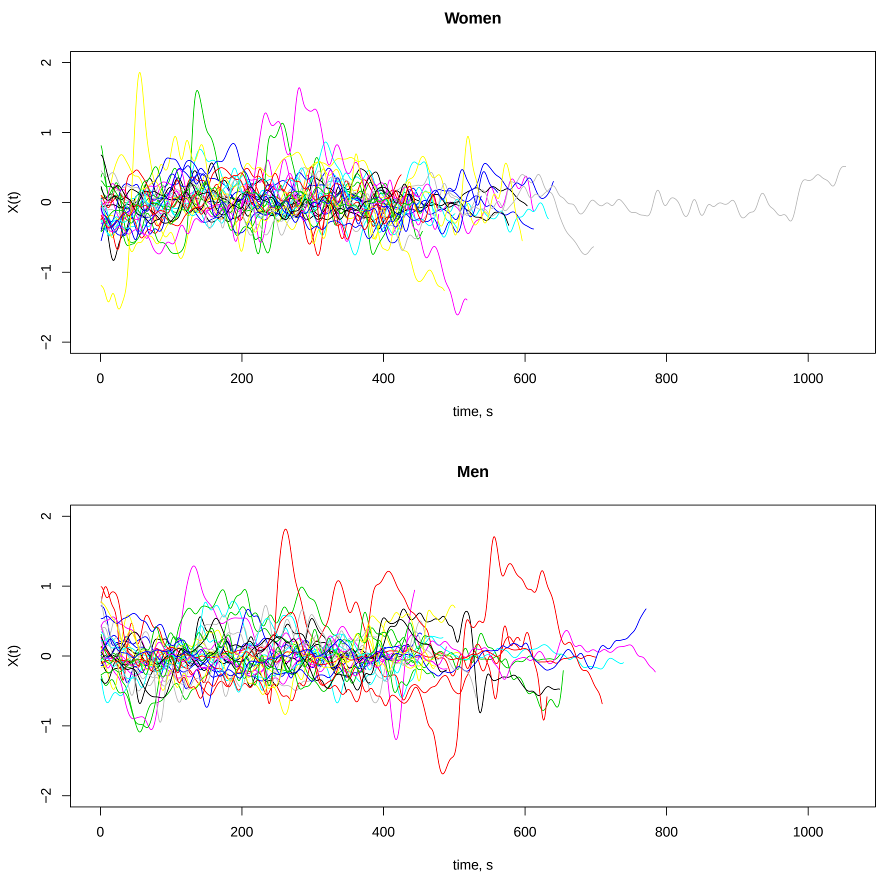

Figure 5: Raw HBO data of all respondents measured with first optode. The plot on the top represents data for all women participated in the experiment, plot on the bottom - data for all men.

Source: created by the author.

4.2 Data smoothing

The smoothing of discrete data points of the fNIRS dataset is challenging due to different lengths of observations. In this paper, ideas presented in Gudan [31, Sections 3.1.1, 3.2.1] and Bartkus [5, Section 5.2.1] are followed in order to obtain a smooth functional data object.

Let us assume that each respondent had to go through the same process during the BCST. Let $y_i(t_{ij})$ represent the changes of concentration of some feature during the BCST, where $i = 1, \ldots, 35$ denotes each respondent participated in the test (taking gender into account) and t_{ij}, $j = 1, \ldots, J_i$, corresponds to time in seconds for every i. Data is smoothed by removing measurement errors and represented as continuous functions of time t. Thus, y_{ij} can be modelled as (4). Let us simplify the notation and denote $y_j = x(t_j) + \epsilon_j$. Then $x(t)$, given $t_j = t$, can be approximated as (5), a linear combination of K basis functions. The decision of the parameter number of basis K has no versatile rule for optimal choice. In general, the more basis functions are selected, the closer the fitted curve will be compared to the discrete raw data points. However, if too many basis functions are selected, the fitted curves may be too rough, thus the data will be overfitted. Besides, since a lot of random errors are included in the curves, the results may become questionable.

Fourier basis system was applied for the fNIRS data due to the periodic nature of the analysed dataset. The discrete data was smoothed using $K = 11$ basis functions. Then, smoothed curves were evaluated over $N = 101$ points $t_l = l/100$, where $l = 0, 1, \dots, 100$, to normalise and transform curves into interval $t \in [0, 1]$ (Figure 6). The nature of the analysed process requires us to use a full measured length of observations for each respondent rather than some explicit part, for instance, first 100 seconds. Thus, the solution of transforming data into an interval $t \in [0, 1]$ is appropriate to deal with the issue of different observation lengths. It is important to note that before mentioned smoothing technique was applied to data of each gender separately to maintain the structure inherent by a specific gender.

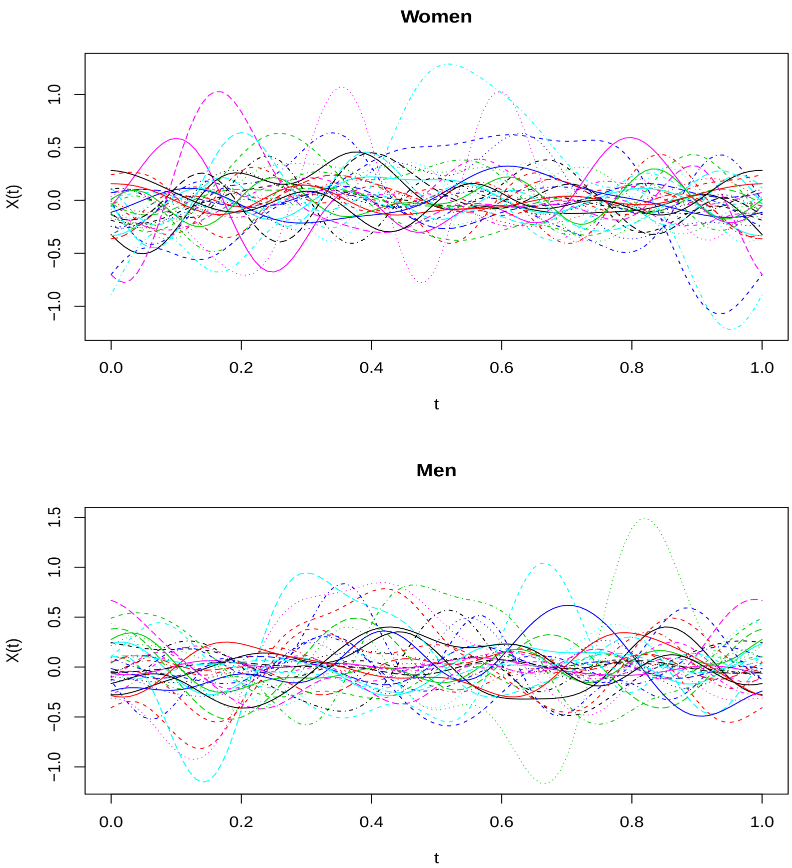

Figure 6: Smoothed HBO data of all respondents measured with first optode. The plot on the top represents data for all women participated in the experiment, plot on the bottom - data for all men.

Source: created by the author.

The commonly used technique of functional continuous registration was attempted to apply on fNIRS data despite a highly varying number of local minima and maxima. However, the method is computationally heavy and did not provide significantly better results in further analysis. Hence, the technique is not under consideration in this thesis.

4.3 Descriptive analysis

A handful of curves outlying in shape were discovered during the explanatory analysis. Shape-outlyingness might be informative and hold essential insights regarding gender. A few observations outlying in the duration of BCST completion visible in Figure 5. Thus, the transformation explained in Section 4.2 solves the issue. Limited amount of respondents measured during the test constrains us. Hence, a thorough analysis of outliers was not considered and the full dataset was employed further.

During the beginning of brain stimulation and the first phase of the hemodynamic response, the demand for oxygen increases, therefore the concentration of oxyhemoglobin raises. The second phase begins when total blood indraught increases due to widening of blood vessels, thus the ratio of deoxyhemoglobin raises and the concentration of oxyhemoglobin starts to decrease.

The mean functions of oxyhemoglobin fluctuations for each gender are presented in Figure 7. At the start of the experiment ratio of the consumed oxyhemoglobin is higher for men but this level drops suddenly and again reaches the peak of the oxyhemoglobin consumption almost halfway of the BCST. The demand for oxygen increases at a slow pace for women. Then, as in the case of men, oxyhemoglobin consumption reaches the peak almost halfway of the experiment. The level of oxyhemoglobin concentration is higher for women throughout almost all exercise time. However, women finish the test with a significantly lower level of oxyhemoglobin consumption than men.

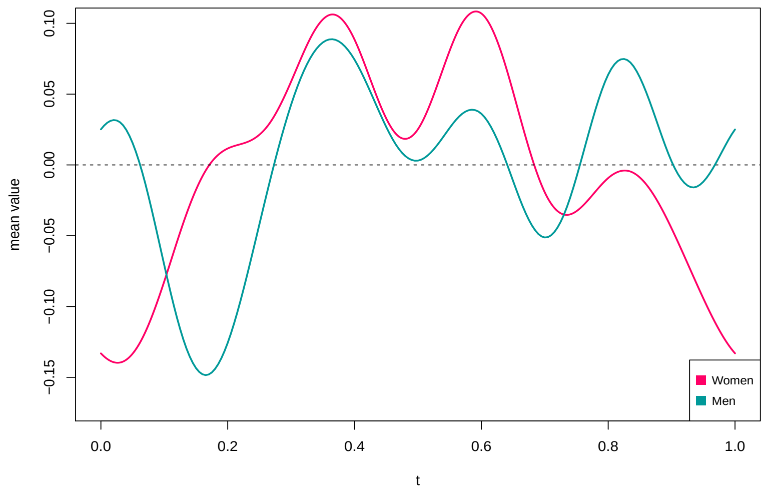

Figure 7: Mean functions of HBO first optode for women and men participated in the experiment.

Source: created by the author.

In Figure 8 the highest depth values of oxyhemoglobin fluctuations for each gender are highlighted. The deepest functions were obtained using five depth notions considered in this paper (see Section 1.3). The functional median provided by the Fraiman and Muniz method has the same pattern as the deepest function obtained by h-mode depth method. While other three methods (the random Tukey depth, the random projection depth and the double random projection depth) are based on the random projections of the curves, slightly different results in shape and amplitude are provided compared to the first two methods. Furthermore, the discrepancy of deepest functions among both genders is not vital in explored cases.

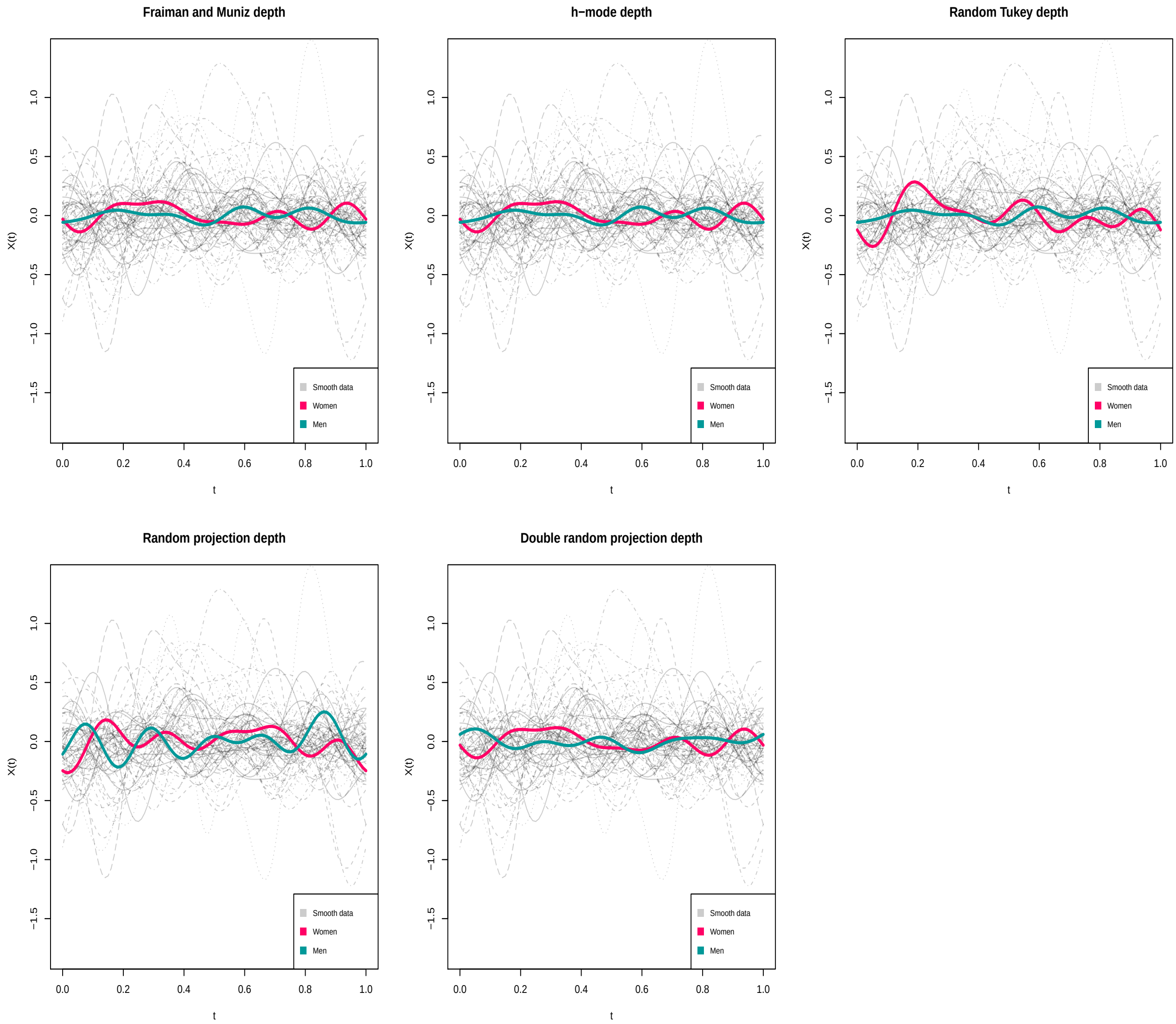

Figure 8: Depth functions of HBO first optode for women and men participated in the experiment.

Source: created by the author.

4.4 Classification algorithm

In this section, smooth fNIRS data (transformed according to the approach described in Section 4.2) is considered for functional depth-based supervised classification. With recent advances in literature functional depth has become a simple, yet powerful, nonparametric tool for classification problems for functional data. Therefore, the performance of supervised functional classification is analysed using five functional depth definitions (see Section 1.3).

Considering sample volume and the special structure of fNIRS data, the concept of a suitable classification algorithm is proposed. The main idea behind the method is that a leave-one-out classification scheme is conducted for each observation pairing of classes $(y_i, g_i)_{i=1,\ldots,n}$ within fNIRS dataset, where y_i is functional hemodynamic response data, g_i are the gender labels of respondents (whether a respondent is man or woman) and $i = 1, \ldots, n$ denote each respondent participated in BCST, in this case $n = 70$. One at a time, for each classification pairing, every observation is taken out of the pooled sample and maximum depth-based classifier (see Section 1.4) is obtained using training subset from pooled sample data excluding left-one-out observation. Then test subset consists only of left-one-out observation which is mapped to the class with higher depth value achieved using the maximum depth-based classifier. All left-one-out observations are classified taking one feature and one optode into account. The procedure is repeated until predictions for each respondent under each optode are collected, that is until every observation has 16 predictions associated with optodes. The algorithm of the described procedure is presented in Algorithm 1. The next step is to gather final predictions for each respondent applying majority voting rule (Algorithm 2), where optodes are the voters. That is, observation is finally assigned to the class where the amount of predicted labels is higher. In the case of ties, observation is classified as "Tie". These steps (Algorithm 1 and Algorithm 2) are repeated for each feature separately while also changing functional depth definition in maximum depth classifier.

The procedure helps to include the whole sample of fNIRS data efficiently, that is, each observation contributes both in training and testing the classifier. Moreover, this approach allows shifting classification method from univariate to multivariate functional data.

Algorithm 1 Maximum depth based supervised classification algorithm with leave-one-out schema.

$depth \leftarrow$ Specific definition of depth evaluation method

$Respondents \leftarrow$ Data pairs $(observations, label)$ of 70 respondents
$Optodes \leftarrow$ 16 optodes

for each $optode \in Optodes$ **do**
  for each $respondent \in Respondents$ **do**
    ▷ Training subset consists of all data except data of the specific respondent:
    $data_{train} \leftarrow (Respondents \setminus respondent)_{observations}$
    $label_{train} \leftarrow (Respondents \setminus respondent)_{label}$

    ▷ Test subset consists of left-one-out observation:
    $data_{test} \leftarrow respondent_{observations}$

    ▷ Maximum depth classifier from `R` library `fda.usc` [3, 23] is used
    to get a prediction for each left-one-out observation of *optode*:
    $respondent_{maxDepthClass,optode} \leftarrow$ `fda.usc::classif.depth(`
      $label_{train}$,
      $data_{train}$,
      $data_{test}$,
      $depth$
    `)$group.pred`

  end for

  ▷ Vector of predictions for each *optode*:
  $Predictions_{optode} \leftarrow Respondents_{maxDepthClass,optode}$

end for
return *Predictions*: A list of predictions for each left-one-out *respondent* and *optode*.

Algorithm 2 Final prediction by majority voting rule.

function MAJORITYRULE(n_{man}, n_{woman})
  if $n_{man} = n_{woman}$ **then**
    return $label_{Tie}$
  end if
  if $n_{man} > n_{woman}$ **then**
    return $label_{Man}$
  else
    return $label_{Woman}$
  end if
end function

$Respondents \leftarrow$ Data pairs $(observations, label)$ of 70 respondents
$Optodes \leftarrow$ 16 optodes

$Predictions \leftarrow$ Predicted values obtained in Algorithm 1: tuples of predicted labels for each of 70 respondents and 16 optodes $(respondent, optode, maxDepthClass)$

▷ Count predicted labels under each *optode* for every *respondent*:
for each $respondent \in Respondents$ **do**
  $n_{man} \leftarrow 0$
  $n_{woman} \leftarrow 0$
  for each $optode \in Optodes$ **do**
    if $Predictions_{respondent,optode} = label_{Man}$ **then**
      $n_{man} \leftarrow n_{man} + 1$
    else
      $n_{woman} \leftarrow n_{woman} + 1$
    end if
  end for
  ▷ Get final prediction for every *respondent* by majority voting:
  $Final\ predictions_{respondent} \leftarrow$ MAJORITYVOTE(n_{man}, n_{woman})
end for
return *Final predictions*: A list of majority vote predictions for each *respondent*.

Results

In this section, results of previously overviewed method applied for the fNIRS data are presented. In addition, k-NN classifier [18] is used for comparison. This method is a simple non-parametric classification alternative easy to apply even with functional data.

Natural way to explore and interpret results is based on the structure of frontal lobe. The first eight optodes represent left brain frontal lobe while the rest describe right brain frontal lobe. Further results are presented by organizing optodes into groups of the whole frontal lobe of 16 optodes, left and right frontal lobe of 8 optodes each, and quarters of optodes.

Tied classification results, when label "man" is assigned to an observation by the same amount of optodes as label "woman", are preserved. The reason is to avoid random label allocation. In the Table 2 results of ties percentage using described classification method (Algorithm 1 and Algorithm 2) for all combinations of feature, depth definition and group of optodes are presented. In Table C.9 (see appendix C), results of ties percentage using k-NN classifier for all combinations of feature and group of optodes are presented. Combinations with at least 20 percent of tied classifications are not considered in further analysis.

Feature	Depth	Optodes 1-16	1-8	9-16	1-4	5-8	9-12	13-16
HBO	FM	2.86	7.14	0	10	18.57	10	10
	hM	0	17.14	0	50	0	50	0
	RT	1.43	1.43	1.43	7.14	7.14	7.14	8.57
	RP	1.43	2.86	1.43	15.71	2.86	15.71	2.86
	RPD	0	1.43	1.43	21.43	8.57	21.43	2.86
HBR	FM	7.14	17.14	15.71	42.86	20	42.86	31.43
	hM	15.71	40	27.14	27.14	35.71	27.14	21.43
	RT	1.43	5.71	2.86	21.43	15.71	21.43	17.14
	RP	14.29	18.57	17.14	51.43	27.14	51.43	27.14
	RPD	2.86	7.14	8.57	15.71	17.14	15.71	22.86
OXY	FM	4.29	22.86	15.71	28.57	28.57	28.57	31.43
	hM	7.14	21.43	12.86	25.71	45.71	25.71	0
	RT	1.43	7.14	7.14	8.57	11.43	8.57	12.86
	RP	12.86	18.57	8.57	21.43	37.14	21.43	18.57
	RPD	5.71	10	14.29	21.43	24.29	21.43	22.86
HBT	FM	1.43	4.29	1.43	22.86	12.86	22.86	5.71
	hM	0	0	0	75.71	1.43	75.71	0
	RT	0	4.29	7.14	12.86	8.57	12.86	12.86
	RP	0	11.43	0	20	14.29	20	1.43
	RPD	0	1.43	0	65.71	4.29	65.71	0

Table 2: Percentage of tied classification results. Highlighted cells represent values greater or equal to 20.

Source: created by the author.

The ability to distinguish between genders is measured by performance metrics such as sensitivity (rate of correctly classified men), specificity (rate of correctly classified women), accuracy (proportion of correctly classified observations overall) and F1 score (harmonic mean of positive predictive values - proportion of correctly classified men and overall observations classified as men - and sensitivity). The classification method (Algorithm 1 and Algorithm 2) is evaluated using these metrics without including tied classifications. The results are summarised in Table 3, Table 4, Table 5 and Table 6 respectively. The performance of k-NN is described in Table C.10, Table C.11, Table C.12 and Table C.13 (see appendix C).

Table 3 suggests that hemodynamic response of men respondents is notably expressed in features of oxyhemoglobin and total blood indraught because of high true positive rates evaluated for the most combinations of depth and optode groups. Though, the sensitivity of deoxyhemoglobin and oxygenation combinations are lower. Opposite results are visible in specificity (Table 4) - HBO and HBT combinations acquire low values, while values for HBR and OXY combinations are slightly higher. Although sensitivity and specificity values using k-NN classifier are quite hight, most of the optodes and feature combinations are not considered due to high ties ratio.

Feature	Depth	Optodes						
		1-16	1-8	9-16	1-4	5-8	9-12	13-16
HBO	FM	1.00	0.97	1.00	0.90	0.94	1.00	1.00
	hM	1.00	0.96	1.00	0.24	1.00	1.00	1.00
	RT	1.00	0.97	1.00	1.00	0.97	1.00	0.97
	RP	1.00	1.00	1.00	1.00	0.97	1.00	0.97
	RPD	1.00	0.97	1.00	0.93	1.00	1.00	0.97
HBR	FM	0.71	0.75	0.65	0.74	0.69	0.80	0.55
	hM	0.59	0.44	0.75	0.74	0.17	0.20	0.81
	RT	1.00	1.00	0.97	1.00	0.97	1.00	0.93
	RP	0.77	0.75	0.85	0.94	0.70	0.96	0.58
	RPD	0.91	0.81	0.91	0.87	0.81	1.00	0.54
OXY	FM	0.64	0.62	0.71	0.79	0.42	0.75	0.65
	hM	0.70	0.54	1.00	0.77	0.24	0.48	1.00
	RT	0.94	0.94	0.94	0.91	0.94	0.97	0.94
	RP	0.87	0.80	0.79	0.90	0.58	0.80	0.87
	RPD	0.76	0.72	0.73	0.87	0.65	0.64	0.79
HBT	FM	1.00	0.94	1.00	0.89	0.97	1.00	1.00
	hM	1.00	0.94	1.00	0.27	1.00	1.00	1.00
	RT	1.00	0.97	1.00	1.00	0.97	1.00	0.97
	RP	1.00	1.00	1.00	0.93	1.00	1.00	1.00
	RPD	1.00	1.00	1.00	1.00	1.00	1.00	1.00

Table 3: Sensitivity (true positive rates) - rates of correctly classified men. Highlighted cells represent values where percentage of tied classification is greater or equal to 20.

Source: created by the author.

Feature	Depth	Optodes						
		1-16	1-8	9-16	1-4	5-8	9-12	13-16
HBO	FM	0.00	0.18	0.00	0.19	0.08	0.00	0.00
	hM	0.00	0.00	0.00	0.44	0.00	0.00	0.00
	RT	0.03	0.03	0.12	0.00	0.07	0.04	0.16
	RP	0.00	0.03	0.00	0.00	0.06	0.00	0.00
	RPD	0.00	0.03	0.00	0.04	0.00	0.00	0.00
HBR	FM	0.47	0.57	0.43	0.47	0.59	0.26	0.58
	hM	0.03	0.06	0.03	0.00	0.59	0.22	0.03
	RT	0.03	0.09	0.03	0.04	0.19	0.06	0.03
	RP	0.31	0.45	0.26	0.35	0.46	0.08	0.44
	RPD	0.03	0.03	0.06	0.00	0.06	0.00	0.46
OXY	FM	0.47	0.57	0.39	0.43	0.63	0.36	0.32
	hM	0.00	0.17	0.00	0.12	0.31	0.39	0.00
	RT	0.15	0.07	0.13	0.07	0.10	0.13	0.14
	RP	0.13	0.19	0.10	0.15	0.28	0.15	0.11
	RPD	0.24	0.19	0.27	0.04	0.37	0.41	0.04
HBT	FM	0.03	0.09	0.00	0.18	0.00	0.03	0.03
	hM	0.00	0.00	0.00	0.83	0.00	0.00	0.00
	RT	0.11	0.15	0.10	0.07	0.16	0.10	0.07
	RP	0.00	0.03	0.00	0.07	0.00	0.00	0.00
	RPD	0.00	0.00	0.00	0.08	0.00	0.00	0.00

Table 4: Specificity (true negative rates) - rates of correctly classified women. Highlighted cells represent values where percentage of tied classification is greater or equal to 20.

Source: created by the author.

Table 5 indicate that the lowest accuracy 0.31 for the classification procedure (Algorithm 1 and Algorithm 2) is evaluated by a combination of HBR feature and h-mode depth method in the whole frontal lobe. The highest accuracy values were achieved by combinations of HBR feature with FM depth method - 0.66, and RP depth method - 0.60, in the left frontal lobe, and with RT depth method - 0.61, in the second quarter of left frontal lobe (a group of optodes from 5 to 8). The highest classification accuracy obtained with k-NN classifier is 0.61 (combinations of HBO feature with the whole frontal lobe and left frontal lobe, and a combination of HBT with left frontal lobe).

Feature	Depth	Optodes						
		1-16	1-8	9-16	1-4	5-8	9-12	13-16
HBO	FM	0.52	0.55	0.50	0.54	0.54	0.53	0.51
	hM	0.50	0.43	0.50	0.34	0.50	0.49	0.50
	RT	0.51	0.51	0.57	0.49	0.55	0.59	0.58
	RP	0.51	0.52	0.51	0.54	0.53	0.51	0.50
	RPD	0.50	0.49	0.49	0.47	0.52	0.50	0.49
HBR	FM	0.59	0.66	0.54	0.54	0.64	0.52	0.56
	hM	0.31	0.29	0.31	0.33	0.38	0.22	0.33
	RT	0.52	0.56	0.49	0.55	0.61	0.53	0.45
	RP	0.55	0.60	0.53	0.65	0.59	0.54	0.51
	RPD	0.47	0.42	0.48	0.44	0.40	0.49	0.50
OXY	FM	0.55	0.59	0.54	0.64	0.52	0.55	0.50
	hM	0.35	0.35	0.43	0.44	0.26	0.44	0.50
	RT	0.55	0.52	0.54	0.50	0.53	0.56	0.56
	RP	0.49	0.51	0.47	0.55	0.46	0.49	0.51
	RPD	0.50	0.46	0.50	0.49	0.51	0.52	0.44
HBT	FM	0.52	0.52	0.51	0.52	0.53	0.53	0.53
	hM	0.50	0.47	0.50	0.47	0.49	0.50	0.50
	RT	0.56	0.57	0.57	0.57	0.58	0.59	0.54
	RP	0.50	0.52	0.50	0.52	0.55	0.52	0.51
	RPD	0.50	0.49	0.50	0.50	0.48	0.50	0.50

Table 5: Accuracy results (proportion of correctly classified observations). Highlighted cells represent values where percentage of tied classification is greater or equal to 20.

Source: created by the author.

Feature	Depth	Optodes						
		1-16	1-8	9-16	1-4	5-8	9-12	13-16
HBO	FM	0.68	0.67	0.67	0.66	0.69	0.69	0.67
	hM	0.67	0.60	0.67	0.26	0.67	0.66	0.67
	RT	0.67	0.67	0.70	0.66	0.70	0.74	0.70
	RP	0.67	0.67	0.67	0.70	0.68	0.67	0.67
	RPD	0.67	0.65	0.66	0.63	0.68	0.67	0.65
HBR	FM	0.62	0.68	0.60	0.69	0.67	0.62	0.53
	hM	0.45	0.42	0.46	0.50	0.22	0.10	0.48
	RT	0.68	0.70	0.65	0.70	0.73	0.68	0.61
	RP	0.64	0.65	0.63	0.73	0.64	0.68	0.55
	RPD	0.63	0.58	0.64	0.61	0.55	0.65	0.51
OXY	FM	0.58	0.59	0.60	0.72	0.48	0.63	0.59
	hM	0.52	0.44	0.60	0.58	0.30	0.50	0.67
	RT	0.68	0.67	0.67	0.65	0.67	0.69	0.69
	RP	0.63	0.63	0.61	0.68	0.56	0.62	0.65
	RPD	0.60	0.58	0.60	0.65	0.57	0.56	0.61
HBT	FM	0.68	0.67	0.67	0.64	0.69	0.69	0.69
	hM	0.67	0.64	0.67	0.40	0.66	0.67	0.67
	RT	0.69	0.70	0.71	0.72	0.70	0.72	0.69
	RP	0.67	0.67	0.67	0.67	0.71	0.69	0.67
	RPD	0.67	0.66	0.67	0.65	0.65	0.67	0.67

Table 6: F1 scores (harmonic mean of classification precision and sensitivity). Highlighted cells represent values where percentage of tied classification is greater or equal to 20.

Source: created by the author.

This implies that the proposed method is slightly more accurate and more effective than k-NN because of a higher value of achieved accuracy and lower ties amount across considered combinations for classification. Moreover, it is possible to discern gender by measuring left frontal lobe (the group of optodes 1-8). Besides, different patterns inherent by gender could be distinguished more accurately by obtaining more data. Combination of deoxyhemoglobin and FM depth method as well as RP and RT methods provide the most suitable results using maximum depth-based classification within analysed fNIRS data.

To give an idea of the computational burden of the different applied depth methods, the computational times of the complete procedure for data of one feature are as follows: FM=30.26 secs, hM=26.41 secs, RT=13.54 mins, RP=19.04 mins and RPD=1.89 hours.

Depths ensemble

It is feasible to extend the proposed classification procedure with an ensemble of considered depth definitions. The Algorithm D.3 (see appendix D) performs steps from Algorithm 1 and Algorithm 2. Then, for each depth notion predictions of optodes voting are collected. That is, each respondent gains 5 predictions associated with depths. Further, predicted labels are counted under each depth for every respondent. Finally, observation is assigned to the class where the amount of predicted labels is higher.

The procedure is flexible in terms of changing a set of depth definitions. Although application of the Algorithm D.3 was attempted for the fNIRS dataset, we did not benefit from it. The procedure provided worse classification performance comparing to classification while employing one depth at the time. Nevertheless, it is recommended to explore the possibility of using a different set of depth notions in the ensemble.

Conclusions

In this thesis, the fNIRS dataset was analysed applying techniques of functional data analysis. The aim was to conclude whether hemodynamic response between women and men is different. The functional depth-based classification algorithm was introduced to discern women and men considering brain activity data measured during the cognitive experiment. The proposed procedure involves maximum depth-based classification approach while also comparing the results of five different functional depth notions. The algorithm helps to include the whole sample of fNIRS data efficiently and allows shifting classification method from univariate to multivariate functional data.

The procedure is suitable for analysed fNIRS dataset with the particular structure of different lengths of observations, list of optodes and obtained features. The results of the proposed method applied for fNIRS data imply that hemodynamic response is different between genders. The reason is that women and men could be discerned applying the algorithm with particular combinations of feature, depth notion and optodes group. In conclusion, the main differences can be found in the left frontal lobe which follows the knowledge of gender influence to existing cognitive studies. Besides, the proposed classification procedure had a higher performance than k-NN classifier used for comparison.

For future research, the proposed classification algorithm could be analysed with a larger sample of respondents to obtain more reliable results. Moreover, the Monte Carlo simulations could be applied for the classifications involving depth approaches based on random projections to obtain more stable results. Furthermore, it is recommended to explore the possibility of using a different set of depth notions in the depths ensemble for the classification.

Acknowledgments

We would like to show our gratitude to Sigita Činčiutė for providing data analysed in this paper. We would also like to thank Karolis Bartkus who provided interesting insights and expertise that assisted in writing this thesis.

References

[1] Biopac Systems Inc. FNIR400. http://www.lintoninst.co.uk/Products/tabid/63/ProdID/661/Language/en-US/FNIR400A__fNIR_Optical_Brain_Imaging_Station_.aspx. Accessed: 2019-11-20.

[2] Package 'fda'. https://cran.r-project.org/web/packages/fda/fda.pdf, . Accessed: 2019-11-29.

[3] Package 'fda.usc'. https://cran.r-project.org/web/packages/fda.usc/fda.usc.pdf, . Accessed: 2019-11-29.

[4] H. Ayaz, M. Cakir, K. Izzetoglu, A. Curtin, P. Shewokis, S. Bunce, and B. Onaral. Monitoring Expertise Development during Simulated UAV Piloting Tasks using Optical Brain Imaging. *IEEE Aerospace Conf.*, March 2012. doi: 10.1109/AERO.2012.6187350.

[5] K. Bartkus. Functional data analysis of fNIRS data. Master's thesis, Vilnius University, 2019.

[6] R. Bartoszyński, D. K. Pearl, and J. Lawrence. A multidimensional goodness-of-fit test based on interpoint distances. *Journal of American Statistical Association*, 92:577–586, 1997.

[7] A. Bozkurt, A. Rosen, H. Rosen, and B. Onaral. A portable near infrared spectroscopy system for bedside monitoring of newborn brain. *BioMedical Engineering OnLine*, 4(1): 29, January 2005.

[8] S. Bunce, M. Izzetoglu, K. Izzetoglu, B. Onaral, and K. Pourrezaei. Functional near-infrared spectroscopy. *IEEE Eng. Med. Biol. Mag.*, 25(4):54–62, 2006.

[9] A. Chakraborty and P. Chaudhuri. On data depth in infinite dimensional spaces. *Annals of the Institute of Statistical Mathematics*, 66:303–324, 2014.

[10] A. Chakraborty and P. Chaudhuri. The spatial distribution in infinite dimensional spaces and related quantiles and depths. *Annals of Statistics*, 42:1203–1231, 2014.

[11] M. Cope. *The application of near infrared spectroscopy to non invasive monitoring of cerebral oxygenation in the newborn infant.* University of London, 1991.

[12] J. A. Cuesta-Albertos and A. Nieto-Reyes. The random Tukey depth. *Computational Statistics and Data Analysis*, 52:4979–4988, 2008.

[13] J. A. Cuesta-Albertos, R. Fraiman, and T. Ransford. Random projections and goodness-of-fit tests in infinite-dimensional spaces. *Bulletin of the Brazilian Mathematical Society*, 37(4):477–501, 2006.

[14] J. A. Cuesta-Albertos, R. Fraiman, and T. Ransford. A Sharp Form of the Cramér–Wold Theorem. *Journal of Theoretical Probability*, 20(2):201–209, 2007.

[15] A. Cuevas and R. Fraiman. On depth measures and dual statistics. a methodology for dealing with general data. *Journal of Multivariate Analysis*, 100:753–766, 2009.

[16] A. Cuevas, M. Febrero, and R. Fraiman. Robust estimation and classification for functional data via projection-based depth notions. *Computational Statistics*, 22:481–496, 2007.

[17] D. Cyranoski. *Neuroscience: thought experiment.* Nature, 2011.

[18] F. Cérou and A. Guyader. Nearest neighbor classification in infinite dimension. *ESAIM: Probability and Statistics*, 10:340–355, 2006.

[19] A. Delaigle and P. Hall. Achieving near perfect classification for functional data. *Journal of the Royal Statistical Society*, 71(2):267–286, 2012.

[20] A. Delaigle, P. Hall, and N. Bathia. Componentwise classification and clustering of functional data. *Biometrika*, 99(2):299–313, 2012.

[21] P. Eling, K. Derckx, and J. Maes. On the historical and conceptual background of the Wisconsin Card Sorting Test. *Brain and Cognition*, 67(3):247–53, August 2008.

[22] L. Ernst, S. Schneider, A.-C. Ehlis, and A. Falgatter. Review: Functional near infrared spectroscopy in psychiatry: a critical review. *J. Near Infrared Spectrosc.*, 20(1):93–105, January 2012.

[23] M. Febrero-Bande and M. de la Fuente. Statistical Computing in Functional Data Analysis: The R Package fda.usc. *Journal of Statistical Software, Articles*, 51(4):1–28, 2012.

[24] M. Ferrari and V. Quaresima. A brief review on the history of human functional near-infrared spectroscopy (fNIRS) development and fields of application. *Neuroimage*, 63 (2):921–935, 2012.

[25] F. Ferraty and P. Vieu. Curves discrimination: a nonparametric functional approach. *Computational Statistics and Data Analysis*, 44:161–173, 2003.

[26] F. Ferraty and P. Vieu. *Nonparametric Functional Data Analysis. Theory and Practice.* Springer, 2006.

[27] R. Fraiman and G. Muniz. Trimmed means for functional data. *Test*, 10(2):419–440, 2001.

[28] A. K. Ghosh and P. Chaudhuri. On maximum depth and related classifiers. *Scandinavian Journal of Statistics*, 32:327–350, 2005.

[29] I. Gijbels and S. Nagy. On a General Definition of Depth for Functional Data. *Statistical Science*, 32(4):630–639, 2017.

[30] E. Goldberg, D. Roediger, N. E. Kucukboyaci, C. Carlson, O. Devinsky, R. Kuzniecky, E. Halgren, and T. Thesen. Hemispheric asymmetries of cortical volume in the human brain. *Cortex*, 49(1):200–10, January 2013.

[31] J. Gudan. Analysis of a Tax Collection Using Functional Data. Master's thesis, Vilnius University, 2017.

[32] S. Helander. On depth based classification of functional data. Master's thesis, Aalto University. School of science, 2018.

[33] F. Homae, H. Watanabe, T. Nakano, and G. Taga. Large-scale brain networks underlying language acquisition in early infancy. *Frontiers in Psychology*, 2:93, January 2011.

[34] K. Hugdahl and R. Westerhausen. *The Two Halves of the Brain.* The MIT Press, 2010.

[35] J. D. Ingle and S. R. Crouch. *Spectrochemical analysis*. Prentice Hall, 1988.

[36] International Union of Pure and Applied Chemistry. *Gold Book*. IUPAC, 1997.

[37] G. M. James and T. J. Hastie. Functional linear discriminant analysis for irregularly sampled curves. *Journal of the Royal Statistical Society*, 63(3):533–550, 2001.

[38] F. Jöbsis. Noninvasive, infrared monitoring of cerebral and myocardial oxygen sufficiency and circulatory parameters. *Science*, 198(4323):1264–1267, 1977.

[39] G. Koshevoy and K. Mosler. Zonoid Trimming for Multivariate Distributions. *The Annals of Statistics*, 25:1998–2017, 1997.

[40] T. Lange, K. Mosler, and P. Mozharovskyi. Fast nonparametric classification based on data depth. *Statistical Papers*, 55(1):49–69, 2014.

[41] R. Liu, J. Parelius, and K. Singh. Multivariate analysis by data depth: descriptive statistics, graphics and inference. *The Annals of Statistics*, 27:783–858, 1999.

[42] R. Y. Liu. On a Notion of Data Depth Based on Random Simplices. *Annals of Statistics*, 18:404–414, 1990.

[43] R. Y. Liu and K. Singh. A quality index based on data depth and multivariate rank tests. *Journal of American Statistical Association*, 88:252–260, 1993.

[44] S. López-Pintado and J. Romo. Depth based classification for functional data. In R. Y. Liu, R. Serfling, and D. L. Souvaine, editors, *DIMACS Series in Discrete Mathematics and Theoretical Computer Science*, volume Data Depth: Robust Multivariate Analysis, Computational Geometry and Applications, pages 103–120. AMS and DIMACS, 2006.

[45] S. López-Pintado and J. Romo. On the concept of depth for functional data. *Journal of the American Statistical Association*, 104:718–734, 2009.

[46] S. López-Pintado and J. Romo. A half-region depth for functional data. *Computational Statistics and Data Analysis*, 55:1679–1695, 2011.

[47] P. C. Mahalanobis. On the generalized distance in statistics. *National Institute of Science of India*, 12:49–55, 1936.

[48] O. Monchi, M. Petrides, V. Petre, K. Worsley, and A. Dagher. Card-sorting revisited: distinct neural circuits participating in different stages of the task identified by event-related fMRI. *The Journal of neuroscience: the official journal of the Society for Neuroscience*, 21(19):7733–41, October 2001.

[49] A. Nieto-Reyes. On the properties of functional depth. In *Recent Advances in Functional Data Analysis and Related Topics: Selected papers from the 2nd International Workshop on Functional and Operatorial Statistics (IWFOS'2011)*, pages 239–244. Physica-Verlag/Springer, Heidelberg, 2011. (F. Ferraty, ed.).

[50] A. Nieto-Reyes and H. Battey. A topologically valid definition of depth for functional data. *Statistical science*, 31:61–79, 2016.

[51] E. Nyhus and F. Barceló. The Wisconsin Card Sorting Test and the cognitive assessment of prefrontal executive functions: A critical update. *Brain and Cognition*, 71(3):437–51, December 2009.

[52] D. Purves. *Neuroscience.* Sinauer Associates, 3rd edition, 2004.

[53] J. Ramsay and B. W. Silverman. *Functional Data Analysis.* New York: Springer, 2nd edition, 2005.

[54] P. J. Rousseeuw and M. Hubert. Regression depth (with discussion). *Journal of American Statistical Association*, 94:388–433, 1999.

[55] R. Serfling. Equivariance and invariance properties of multivariate quantile and related functions, and the role of standardisation. *Journal of Nonparametric Statistics*, 22(7): 915–936, 2010.

[56] T. Sun and C. Walsh. Molecular approaches to brain asymmetry and handedness. *Nature Reviews Neuroscience*, 2006.

[57] A. Toga and P. Thompson. Mapping brain asymmetry. *Nature Reviews Neuroscience*, 2003.

[58] J. W. Tukey. Mathematics and the picturing of data. In *Proceedings of the International Congress of Mathematicians (Vancouver, B. C., 1974)*, volume 2, pages 523–531. Canad. Math. Congress, Montreal, Que., 1975.

[59] A. W. van der Vaart and J. A. Wellner. *Weak convergence and empirical processes: with applications to statistics.* Springer Series in Statistics, Springer-Verlag, New York, 1996.

[60] Y. Vardi and C.-H. Zhang. The multivariate l_1-Median and Associated Data Depth. *Proceedings of the National Academy of Sciences*, 97(4):1423–1426, 1999.

[61] J. Wang, B. Cao, X. Cai, H. Gao, and F. Li. Brain Activation of Negative Feedback in Rule Acquisition Revealed in a Segmented Wisconsin Card Sorting Test. *PLOS ONE*, October 2015. doi: https://doi.org/10.1371/journal.pone.0140731.

[62] H. Zhu, P. J. Brown, and J. S. Morris. Robust classification of functional and quantitative image data using functional mixed models. *Biometrics*, 68(4):1260–1268, 2012.

[63] Y. Zuo and R. Serfling. General notions of statistical depth function. *Annals of Statistics*, 28:461–482, 2000.

[64] Y. Zuo and R. Serfling. Nonparametric notions of multivariate "scatter measure" and "more scattered" based on statistical depth functions. *Journal of Multivariate Analysis*, 75:62–78, 2000.

[65] S. Činčiūtė. Lyties ir rankiškumo įtaka kaktinės žmogaus smegenų žievės hemodinamikai Bergo kortų rūšiavimo testo metu: tyrimas fNIRS metodu. Master's thesis, Vilnius University, 2015.

Appendices

A Confusion matrices of the classification algorithm

Feature	Depth	Predicted class	Optodes 1-16		1-8		9-16		1-4		5-8		9-12		13-16	
		True class	M	W	M	W	M	W	M	W	M	W	M	W	M	W
HBO	FM	M	35	33	30	28	35	35	28	26	29	24	35	31	32	31
		W	0	0	1	6	0	0	3	6	2	2	0	0	0	0
		T	0	2	4	1	0	0	4	3	4	9	0	4	3	4
	hM	M	35	35	25	32	35	35	4	10	35	35	34	35	35	35
		W	0	0	1	0	0	0	13	8	0	0	0	0	0	0
		T	0	0	9	3	0	0	18	17	0	0	1	0	0	0
	RT	M	34	34	34	33	35	30	32	33	34	28	35	25	32	26
		W	0	1	1	1	0	4	0	0	1	2	0	1	1	5
		T	1	0	0	1	0	1	3	2	0	5	0	9	2	4
	RP	M	35	34	34	33	35	34	32	27	34	31	35	34	34	33
		W	0	0	0	1	0	0	0	0	1	2	0	0	1	0
		T	0	1	1	1	0	1	3	8	0	2	0	1	0	2
	RPD	M	35	35	33	34	34	35	25	27	33	31	35	35	33	34
		W	0	0	1	1	0	0	2	1	0	0	0	0	1	0
		T	0	0	1	0	1	0	8	7	2	4	0	0	1	1
HBR	FM	M	22	18	21	13	20	16	17	9	20	11	20	20	12	11
		W	9	16	7	17	11	12	6	8	9	16	5	7	10	15
		T	4	1	7	5	4	7	12	18	6	8	10	8	13	9
	hM	M	17	29	11	16	15	30	17	28	4	9	1	14	17	33
		W	12	1	14	1	5	1	6	0	19	13	4	4	4	1
		T	6	5	10	18	15	4	12	7	12	13	30	17	14	1
	RT	M	35	33	34	29	32	34	29	25	31	22	33	31	25	30
		W	0	1	0	3	1	1	0	1	1	5	0	2	2	1
		T	0	1	1	3	2	0	6	9	3	8	2	2	8	4
	RP	M	24	20	21	16	23	23	16	11	19	13	27	24	15	14
		W	7	9	7	13	4	8	1	6	8	11	1	2	11	11
		T	4	6	7	6	8	4	18	18	8	11	7	9	9	10
	RPD	M	31	33	26	32	29	30	26	29	21	30	33	35	14	15
		W	3	1	6	1	3	2	4	0	5	2	0	0	12	13
		T	1	1	3	2	3	3	5	6	9	3	2	0	9	7
OXY	FM	M	21	18	16	12	20	19	23	12	11	9	21	18	17	15
		W	12	16	10	16	8	12	6	9	15	15	7	10	9	7
		T	2	1	9	7	7	4	6	14	9	11	7	7	9	13
	hM	M	23	32	14	24	26	35	20	23	6	9	12	11	35	35
		W	10	0	12	5	0	0	6	3	19	4	13	7	0	0
		T	2	3	9	6	9	0	9	9	10	22	10	17	0	0
	RT	M	33	29	32	29	31	28	30	29	30	27	31	27	30	25
		W	2	5	2	2	2	4	3	2	2	3	1	4	2	4
		T	0	1	1	4	2	3	2	4	3	5	3	4	3	6
	RP	M	26	27	24	22	27	27	26	22	15	13	24	23	26	24
		W	4	4	6	5	7	3	3	4	11	5	6	4	4	3
		T	5	4	5	8	1	5	6	9	9	17	5	8	5	8
	RPD	M	25	25	23	25	22	22	26	24	17	17	16	16	23	24
		W	8	8	9	6	8	8	4	1	9	10	9	11	6	1
		T	2	2	3	4	5	5	5	10	9	8	10	8	6	10
HBT	FM	M	35	33	32	30	35	34	23	23	32	28	35	32	34	31
		W	0	1	2	3	0	0	3	5	1	0	0	1	0	1
		T	0	1	1	2	0	1	9	7	2	7	0	2	1	3
	hM	M	35	35	33	35	35	35	3	1	34	35	35	35	35	35
		W	0	0	2	0	0	0	8	5	0	0	0	0	0	0
		T	0	0	0	0	0	0	24	29	1	0	0	0	0	0
	RT	M	35	31	33	28	34	28	33	26	32	26	34	26	31	27
		W	0	4	1	5	0	3	0	2	1	5	0	3	1	2
		T	0	0	1	2	1	4	2	7	2	4	1	6	3	6
	RP	M	35	35	31	30	35	35	27	25	33	27	35	32	35	34
		W	0	0	0	1	0	0	2	2	0	0	0	0	0	0
		T	0	0	4	4	0	0	6	8	2	8	0	3	0	1
	RPD	M	35	35	34	35	35	35	11	12	32	35	35	35	35	35
		W	0	0	0	0	0	0	0	1	0	0	0	0	0	0
		T	0	0	1	0	0	0	24	22	3	0	0	0	0	0

Table A.7: Confusion matrices of classification results with all possible combinations of feature, depth and optodes group. M - men, W - women, T - ties.

Source: created by the author.

B Confusion matrices of k-NN classifier

Feature	Predicted class	Optodes 1-16		1-8		9-16		1-4		5-8		9-12		13-16	
		True class													
		M	W	M	W	M	W	M	W	M	W	M	W	M	W
HBO	M	11	5	14	10	7	2	13	8	12	4	7	1	5	3
	W	19	27	12	21	24	28	16	16	13	18	20	23	23	24
	T	5	3	9	4	4	5	6	11	10	13	8	11	7	8
HBR	M	8	12	10	9	8	10	11	8	8	10	6	8	8	12
	W	20	17	12	18	19	14	9	16	11	14	19	16	12	10
	T	7	6	13	8	8	11	15	11	16	11	10	11	15	13
OXY	M	11	13	12	13	7	9	13	8	11	10	10	8	6	7
	W	20	20	17	15	21	18	17	13	14	11	15	14	19	18
	T	4	2	6	7	7	8	5	14	10	14	10	13	10	10
HBT	M	8	5	11	7	8	5	10	12	12	5	9	4	7	4
	W	23	29	15	24	24	27	12	16	17	21	21	23	20	25
	T	4	1	9	4	3	3	13	7	6	9	5	8	8	6

Table B.8: Confusion matrices of k-NN classification results with all possible combinations of feature and optodes group. M - men, W - women, T - ties.

Source: created by the author.

C Performance of k-NN classifier

Feature	Optodes 1-16	1-8	9-16	1-4	5-8	9-12	13-16
HBO	11.43	18.57	12.86	24.29	32.86	24.29	21.43
HBR	18.57	30.00	27.14	37.14	38.57	37.14	40.00
OXY	8.57	18.57	21.43	27.14	34.29	27.14	28.57
HBT	7.14	18.57	8.57	28.57	21.43	28.57	21.43

Table C.9: Percentage of tied classification results with k-NN classifier. Highlighted cells represent values greater or equal to 20.

Source: created by the author.

Feature	Optodes 1-16	1-8	9-16	1-4	5-8	9-12	13-16
HBO	0.37	0.54	0.23	0.45	0.48	0.26	0.18
HBR	0.29	0.46	0.30	0.55	0.42	0.24	0.40
OXY	0.36	0.41	0.25	0.43	0.44	0.40	0.24
HBT	0.26	0.42	0.25	0.46	0.41	0.30	0.26

Table C.10: Sensitivity (true positive rates) - rates of correctly classified men - of k-NN classifier. Highlighted cells represent values where percentage of tied classification is greater or equal to 20.

Source: created by the author.

Feature	Optodes 1-16	1-8	9-16	1-4	5-8	9-12	13-16
HBO	0.84	0.68	0.93	0.67	0.82	0.96	0.89
HBR	0.59	0.67	0.58	0.67	0.58	0.67	0.46
OXY	0.61	0.54	0.67	0.62	0.52	0.64	0.72
HBT	0.85	0.77	0.84	0.57	0.81	0.85	0.86

Table C.11: Specificity (true negative rates) - rates of correctly classified women - of k-NN classifier. Highlighted cells represent values where percentage of tied classification is greater or equal to 20.

Source: created by the author.

Feature	Optodes						
	1-16	1-8	9-16	1-4	5-8	9-12	13-16
HBO	0.61	0.61	0.57	0.55	0.64	0.59	0.53
HBR	0.44	0.57	0.43	0.61	0.51	0.45	0.43
OXY	0.48	0.47	0.46	0.51	0.48	0.51	0.48
HBT	0.57	0.61	0.55	0.52	0.60	0.56	0.57

Table C.12: Accuracy results (proportion of correctly classified observations) with k-NN classifier. Highlighted cells represent values where percentage of tied classification is greater or equal to 20.

Source: created by the author.

Feature	Optodes						
	1-16	1-8	9-16	1-4	5-8	9-12	13-16
HBO	0.48	0.56	0.35	0.52	0.59	0.40	0.28
HBR	0.33	0.49	0.36	0.56	0.43	0.31	0.40
OXY	0.40	0.44	0.32	0.51	0.48	0.47	0.32
HBT	0.36	0.50	0.36	0.46	0.52	0.42	0.37

Table C.13: F1 scores (harmonic mean of classification precision and sensitivity) of k-NN classifier. Highlighted cells represent values where percentage of tied classification is greater or equal to 20.

Source: created by the author.

D Algorithm of depths ensemble

Algorithm D.3 Extension of the classification procedure with depths ensemble.

function MajorityRule($n_{woman}, n_{man}, n_{tie}$)
  if $n_{man} > n_{woman}$ **and** $n_{man} > n_{tie}$ **then**
    return $label_{Man}$
  else if $n_{woman} > n_{man}$ **and** $n_{woman} > n_{tie}$ **then**
    return $label_{Woman}$
  else
    return $label_{Tie}$
  end if
end function

$Depths \leftarrow \{FM, hM, RT, RP, RPD\}$

for each $depth \in Depths$ **do**
  $Predictions_{depth} \leftarrow$ Complete Algorithm 2 with definition $depth$
  ▷ $Predictions_{depth}$ is a list of labels either "Man", "Woman" or "Tie" predicted for each respondent.
end for

▷ Count predicted labels under each $depth$ for every respondent:
for each $prediction \in Predictions$ **do**
  $n_{woman} \leftarrow 0$
  $n_{man} \leftarrow 0$
  $n_{tie} \leftarrow 0$
  for each $depth \in Depths$ **do**
    $n_{(prediction_{depth}\ label)} \leftarrow n_{(prediction_{depth}\ label)} + 1$
  end for

  ▷ Assign observation to the class where amount of predicted labels is higher:
  $prediction_{ensemble\ label} \leftarrow$ MajorityVote($n_{woman}, n_{man}, n_{tie}$)
end for
return $Predictions$: A list of ensemble predictions.